Introduction to optical/IR interferometry

History and basic principles

J. Surdej

Institute of Astrophysics and Geophysics
Liège University
Allée du 6 Août 19c, 4000 Liège, Belgium

E-mail: jsurdej@ulg.ac.be

ESO (Paranal, Chile), 30 July & 1 August 2018

Table of Contents

LIÈGE université

Table of Contents

LIÈGE université

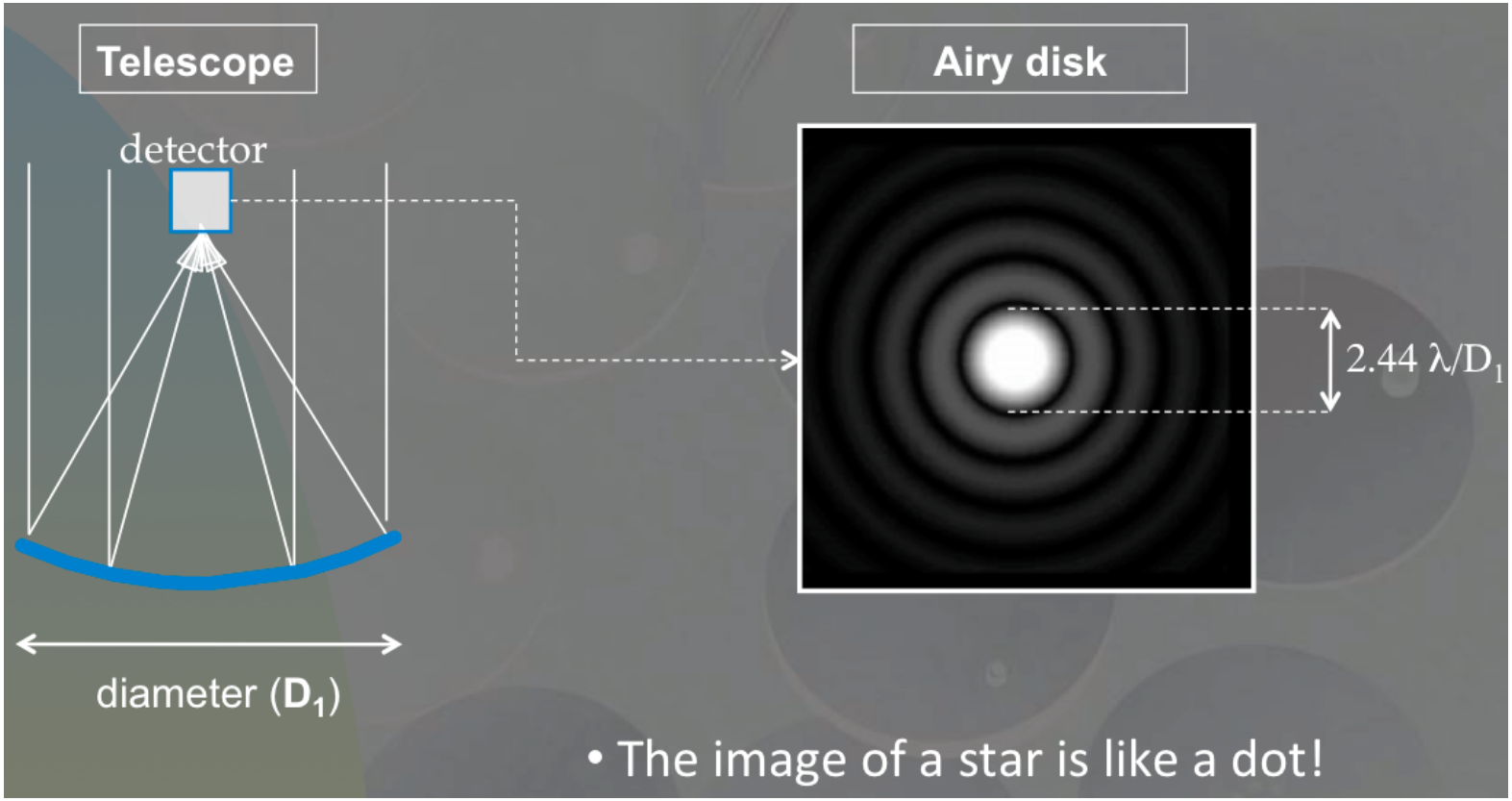

Figure: Airy disk of a point-like star recorded in the focal plane of a telescope with diameter D_1. The angular diameter of the Airy disk is 2.44 λ/D_1.

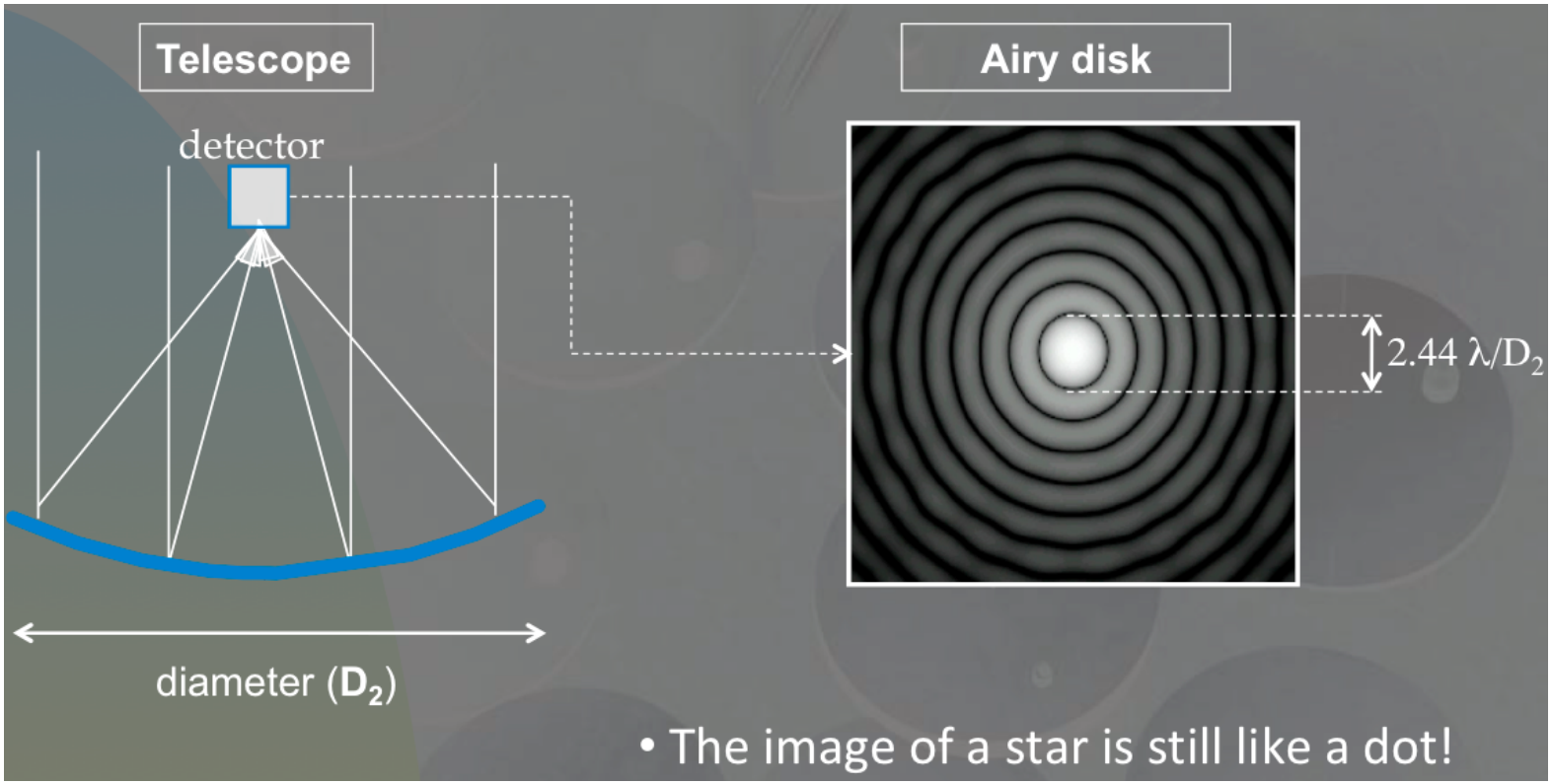

Figure: As the diameter of a telescope increases ($D_2 > D_1$), the Airy disk of a point-like star gets smaller.

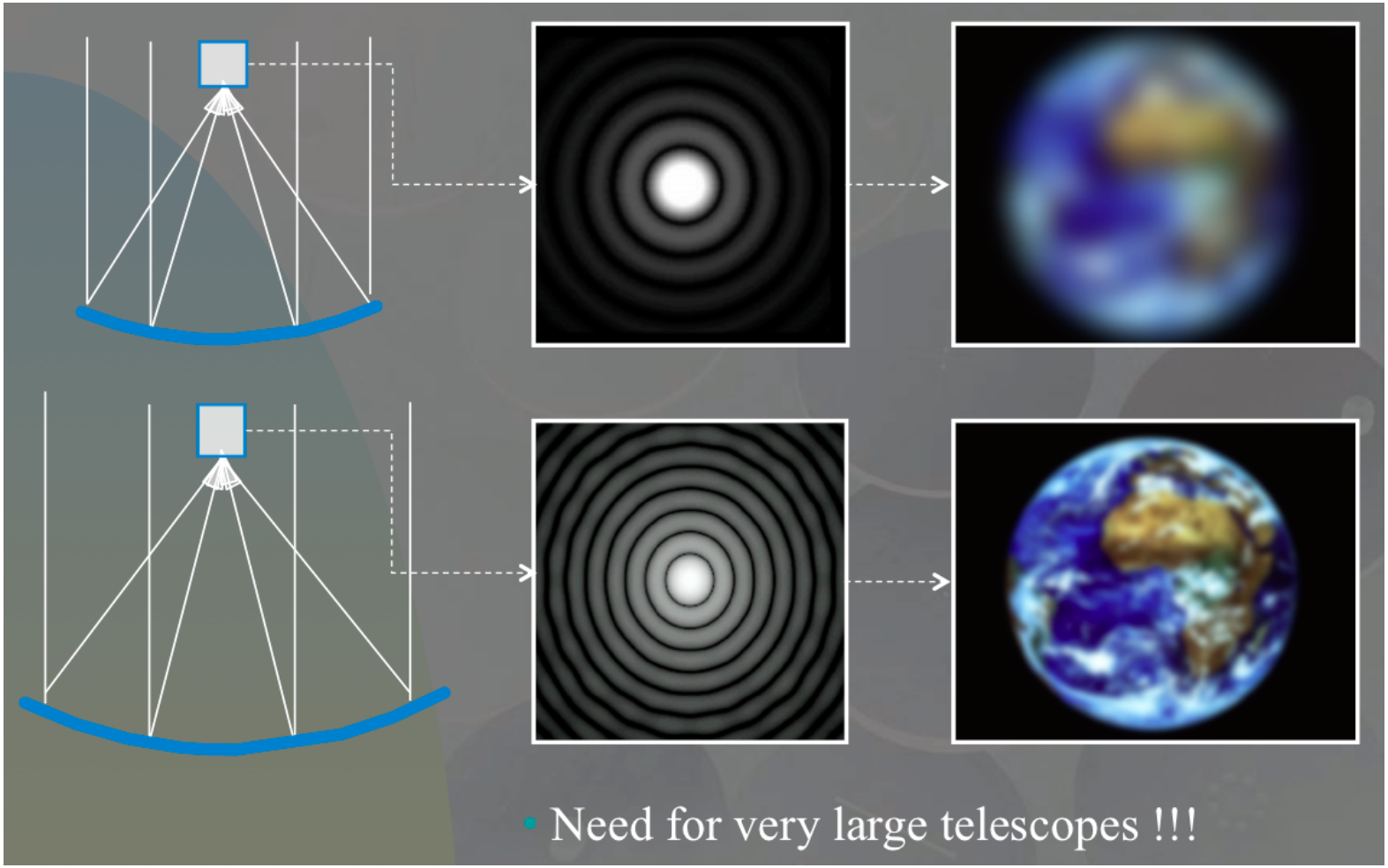

Figure: While observing an extended celestial object (cf. an Earth-like planet) above the atmosphere, we see more details as the diameter of the telescope increases.

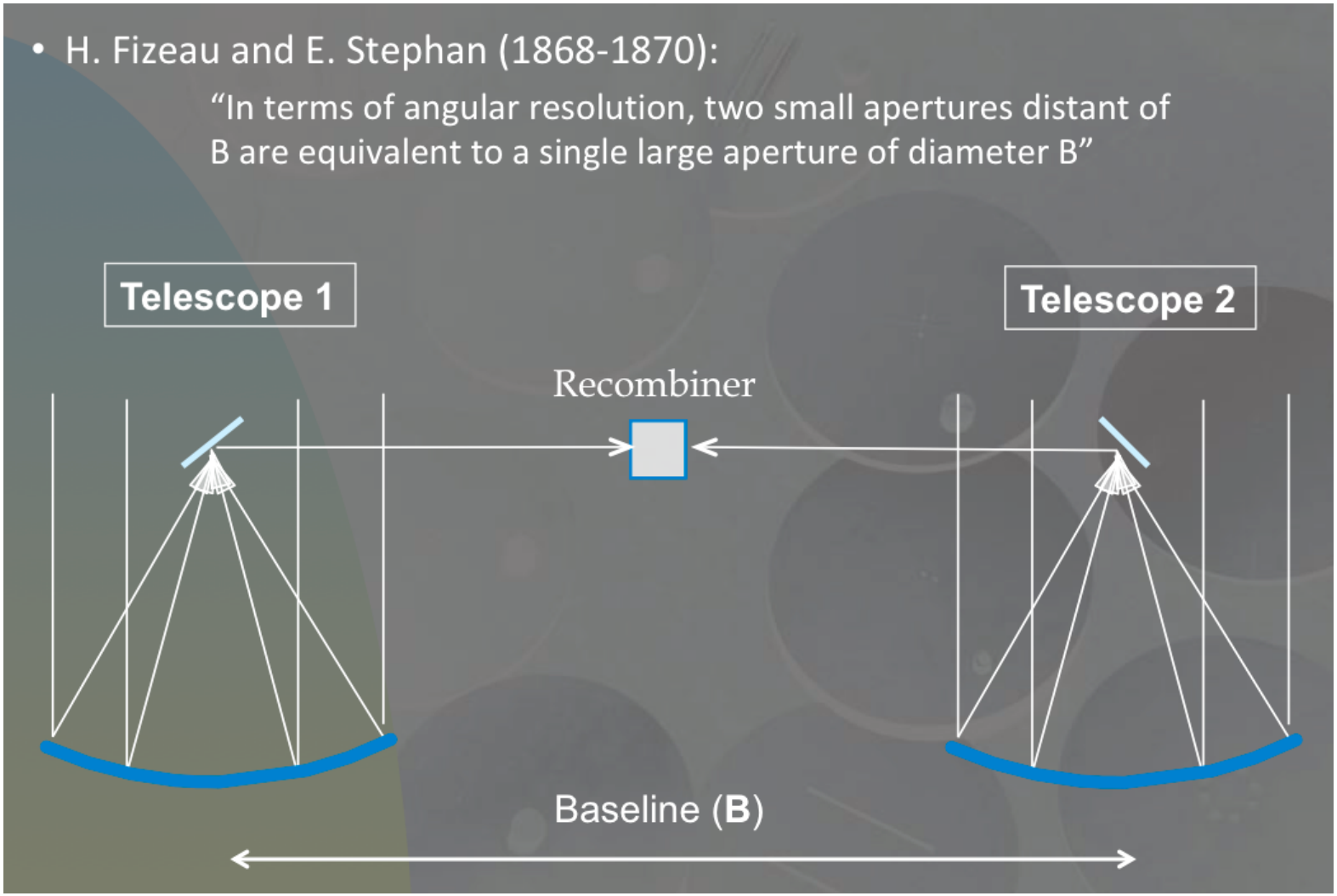

Figure: Fizeau and Stephan proposed to recombine the light from two independent telescopes separated by a baseline B to recover the same angular resolution as that given by a single dish telescope having a diameter B.

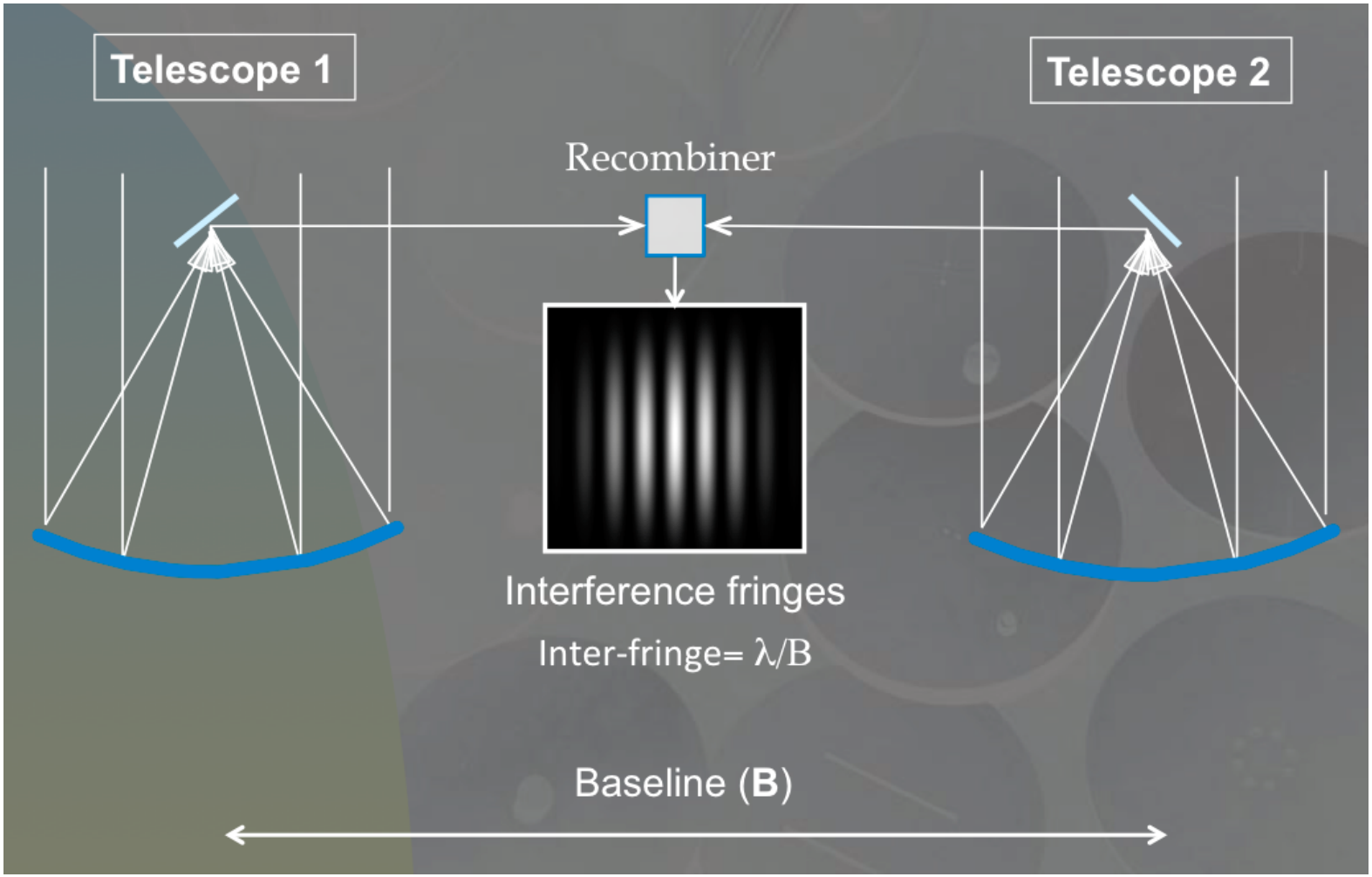

Figure: When recombining the monochromatic light of two independent telescopes, there results the formation of a pattern of bright and dark fringes superimposed over the combined Airy disk. The angular inter-fringe separation is equal to λ/B.

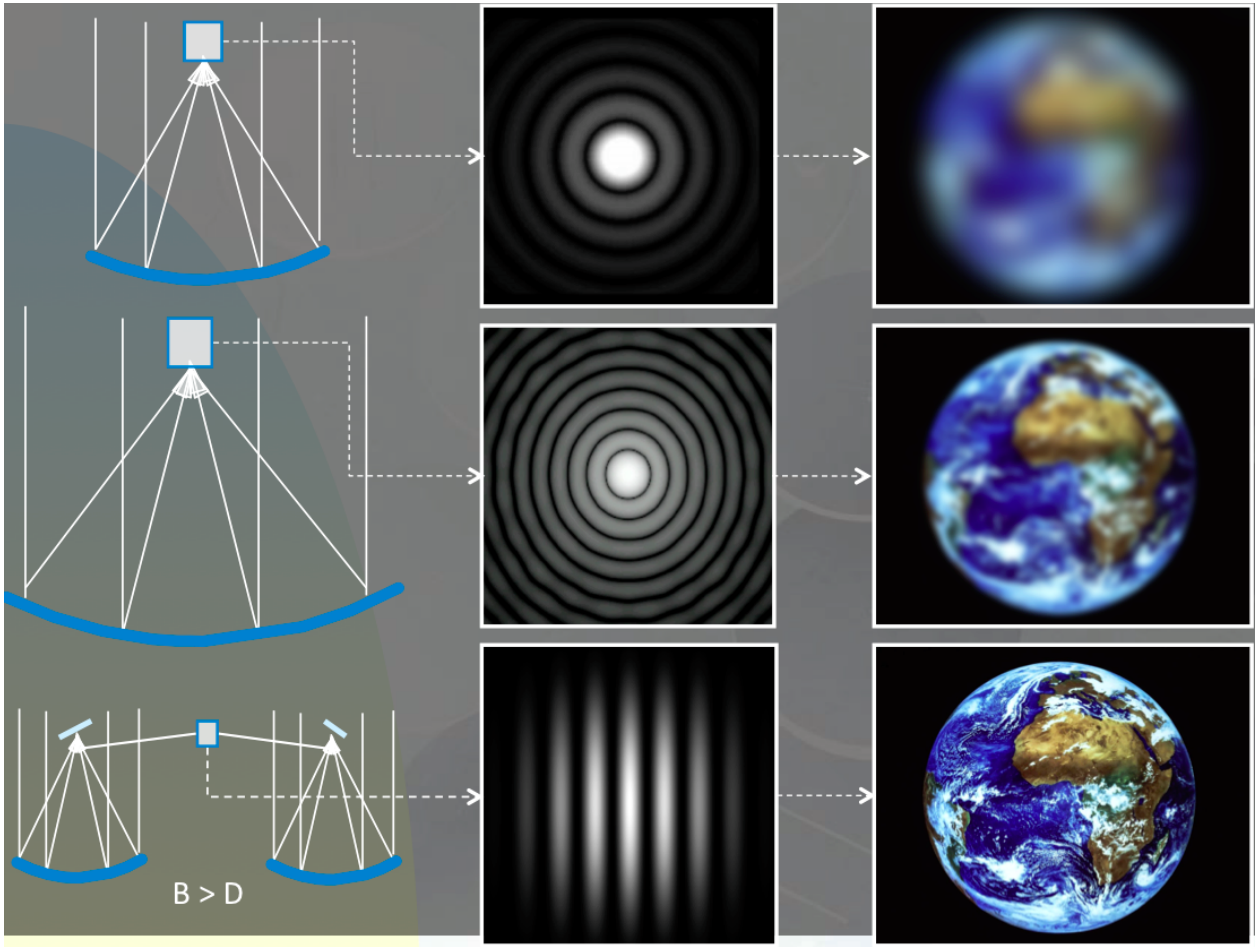

Figure: Improvement expected in angular resolution while observing an extended celestial source (cf. an Earth-like planet) with telescopes of increasing size ($D_2 > D_1$) and with an interferometer composed of two telescopes separated by a baseline $B > D$.

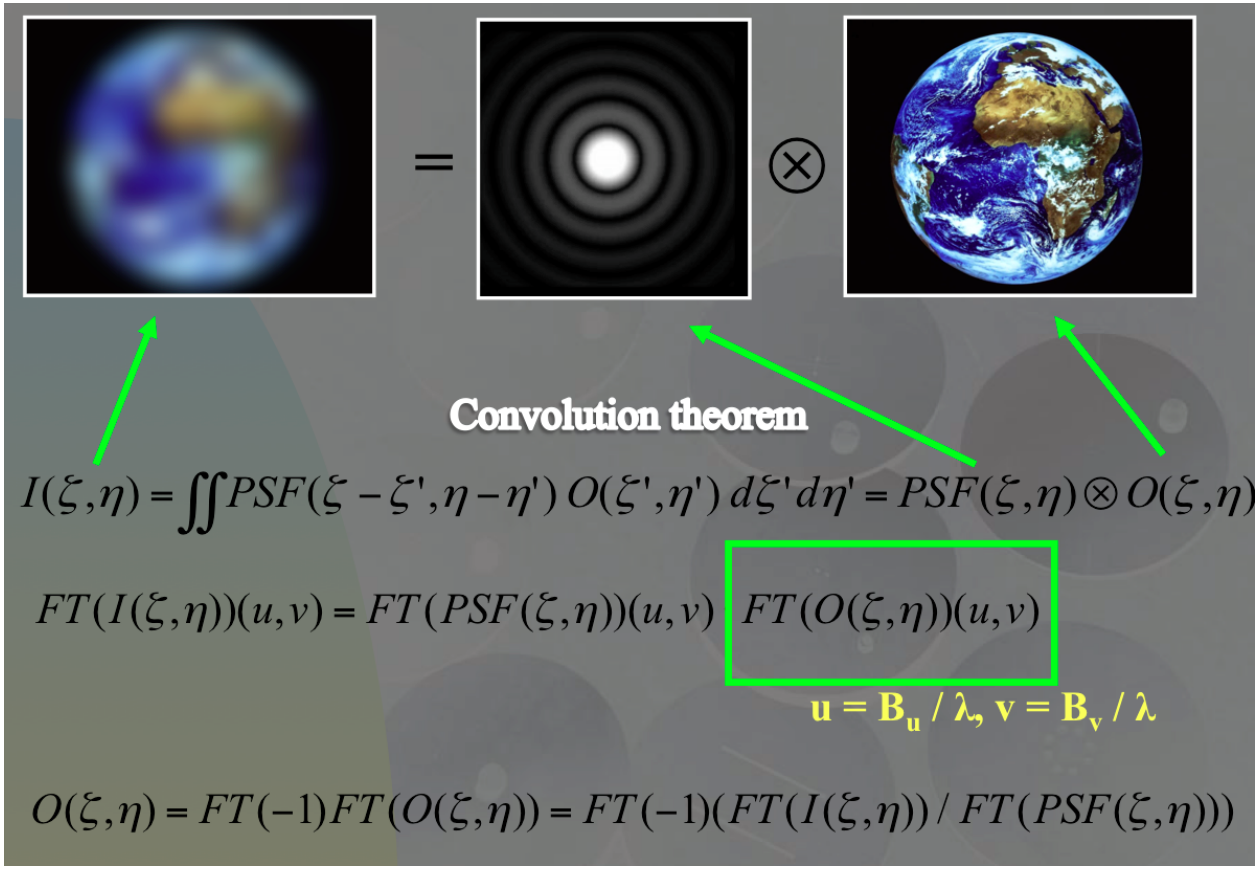

Figure: The image $I(\zeta, \eta)$ we observe in the focal plane of an instrument (cf. single dish telescope) from a distant extended source as a function of its angular coordinates ζ, η is the convolution product of the real source image (cf. the extended Earth-like planet, $O(\zeta, \eta)$) by the point spread function $PSF(\zeta, \eta)$ of the telescope.

Table of Contents

Some reminders

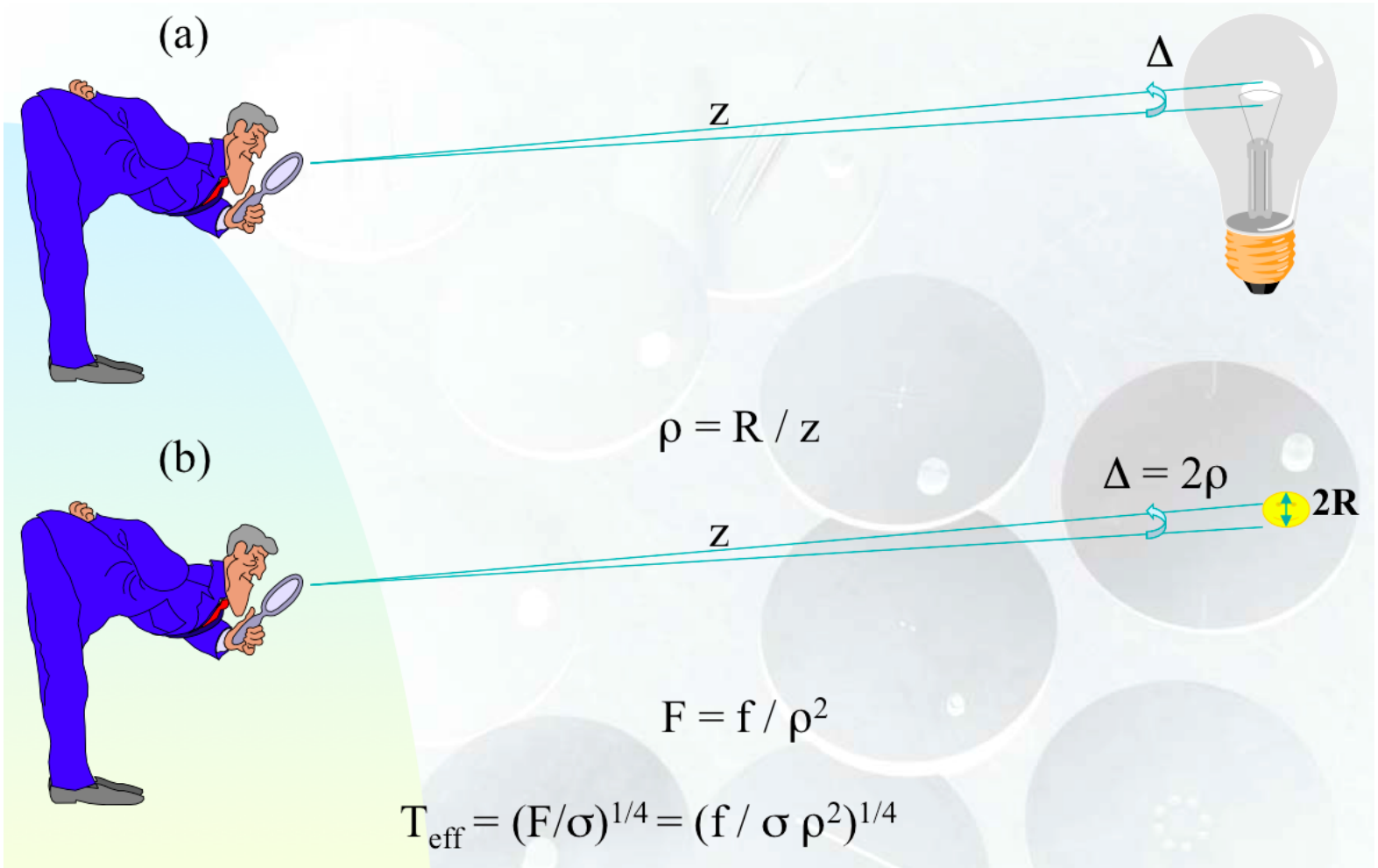

Figure: Resolving the angular diameter of a star (b) is alike trying to estimate the angular size of the filament of a light bulb (a).

Some reminders: Complex representation of an electromagnetic wave

$$E = a\ cos(2\pi(\nu t - z/\lambda)) \tag{1}$$

where

$$\lambda = c\ T = c/\nu \tag{2}$$

c, λ, ν, T and a representing the speed of light, the wavelength, the frequency, the period and the amplitude of the electromagnetic vibrations, respectively (see Figure 9).

Some reminders: Complex representation of an electromagnetic wave

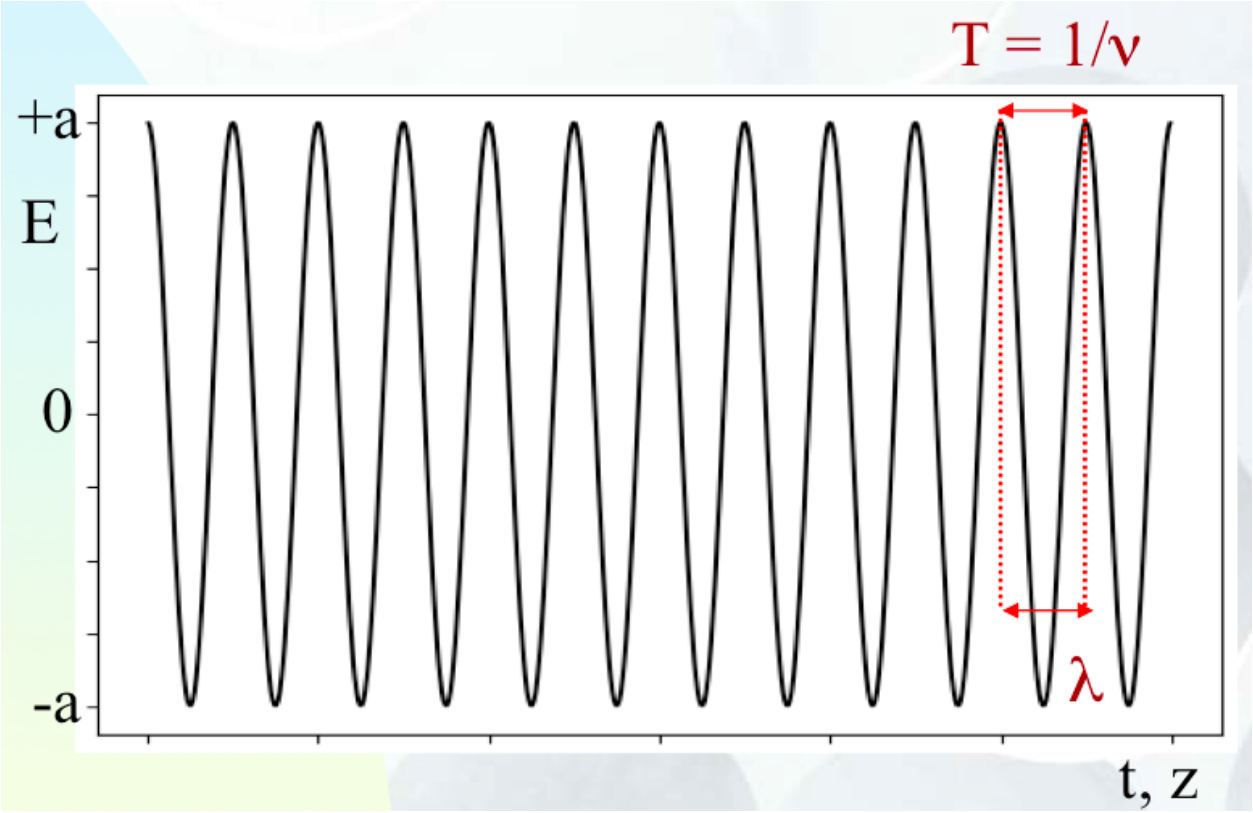

Figure: Representation of an electromagnetic wave.

Some reminders: Complex representation of an electromagnetic wave

We know how convenient it is to rewrite the previous relation in complex notation:

$$E = Re\{a \exp[i2\pi(\nu t - z/\lambda)]\} \tag{3}$$

where Re represents the real part of the expression between the two curly braces.

Some reminders: Complex representation of an electromagnetic wave

We know how convenient it is to rewrite the previous relation in complex notation:

$$E = Re\{a \exp[i2\pi(\nu t - z/\lambda)]\} \tag{3}$$

where Re represents the real part of the expression between the two curly braces.

$$E = a \exp(-i\phi) \exp(i2\pi\nu t) \tag{4}$$

where

$$\phi = 2\pi z/\lambda. \tag{5}$$

Some reminders: Complex representation of an electromagnetic wave

We know how convenient it is to rewrite the previous relation in complex notation:

$$E = Re\{a \exp[i2\pi(\nu t - z/\lambda)]\} \tag{3}$$

where Re represents the real part of the expression between the two curly braces.

$$E = a \exp(-i\phi) \exp(i2\pi\nu t) \tag{4}$$

where

$$\phi = 2\pi z/\lambda. \tag{5}$$

We can then rewrite the previous equation as follows:

$$E = A \exp(i2\pi\nu t), \tag{6}$$

Some reminders: Complex representation of an electromagnetic wave

We know how convenient it is to rewrite the previous relation in complex notation:

$$E = Re\{a \exp[i2\pi(\nu t - z/\lambda)]\} \tag{3}$$

where Re represents the real part of the expression between the two curly braces.

$$E = a \exp(-i\phi) \exp(i2\pi\nu t) \tag{4}$$

where

$$\phi = 2\pi z/\lambda. \tag{5}$$

We can then rewrite the previous equation as follows:

$$E = A \exp(i2\pi\nu t), \tag{6}$$

where

$$A = a \exp(-i\phi) \tag{7}$$

Some reminders: Complex representation of an electromagnetic wave

We know how convenient it is to rewrite the previous relation in complex notation:

$$E = Re\{a \exp[i2\pi(\nu t - z/\lambda)]\} \tag{3}$$

where Re represents the real part of the expression between the two curly braces.

$$E = a \exp(-i\phi) \exp(i2\pi\nu t) \tag{4}$$

where

$$\phi = 2\pi z/\lambda. \tag{5}$$

We can then rewrite the previous equation as follows:

$$E = A \exp(i2\pi\nu t), \tag{6}$$

where

$$A = a \exp(-i\phi) \tag{7}$$

with A representing the complex amplitude of the vibration.

The intensity I is proportional to the temporal average of the square of the electric field:

$$\left\langle E^2 \right\rangle = lim_{T\to\infty} \frac{1}{2T} \int_{-T}^{+T} E^2 dt, \tag{8}$$

The intensity I is proportional to the temporal average of the square of the electric field:

$$\left\langle E^2 \right\rangle = lim_{T\to\infty} \frac{1}{2T} \int_{-T}^{+T} E^2 dt, \tag{8}$$

which is reduced to (e.g. replace in the previous relation E by Eq.(1))

$$\left\langle E^2 \right\rangle = \frac{a^2}{2}, \tag{9}$$

where a is the real amplitude of the electric field.

The intensity I is proportional to the temporal average of the square of the electric field:

$$\left\langle E^2 \right\rangle = lim_{T\to\infty} \frac{1}{2T} \int_{-T}^{+T} E^2 dt, \tag{8}$$

which is reduced to (e.g. replace in the previous relation E by Eq.(1))

$$\left\langle E^2 \right\rangle = \frac{a^2}{2}, \tag{9}$$

where a is the real amplitude of the electric field.
By convention, the intensity of the radiation is defined by the following relation:

$$I = A\ A^* = |A|^2 = a^2. \tag{10}$$

Some reminders: Principle of Huygens-Fresnel

$\sigma = 2.44\ \lambda / d$

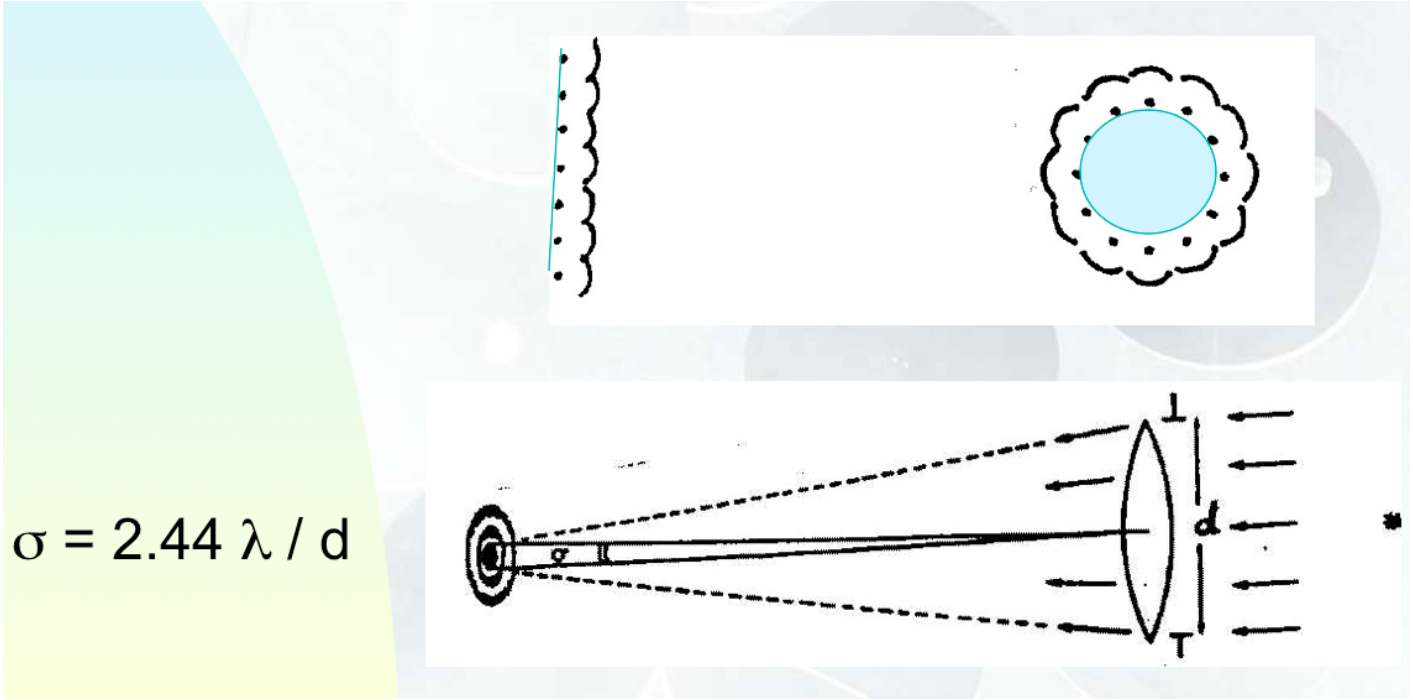

Figure: Illustration of the Huygens-Fresnel principle during the propagation of a plane or circular wavefront and diffraction of light which encounters a converging lens.

Some reminders: Principle of Huygens-Fresnel

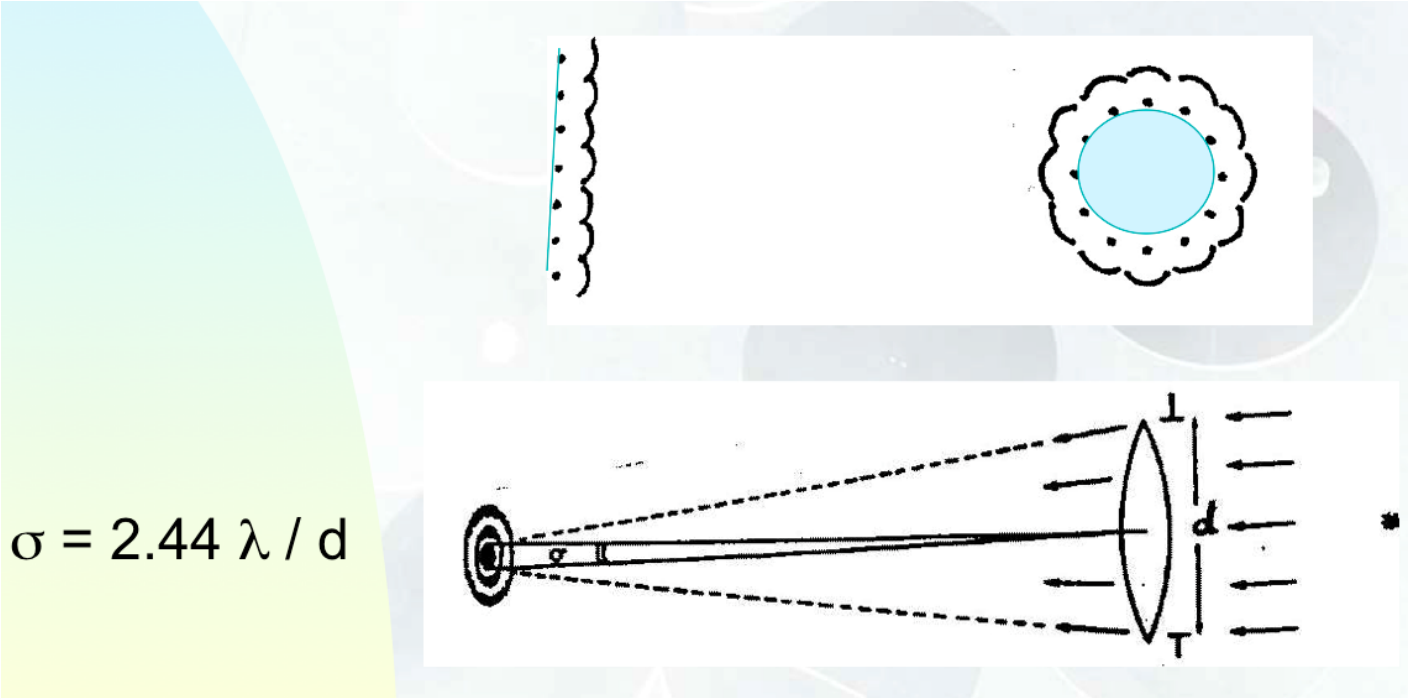

Figure: Illustration of the Huygens-Fresnel principle during the propagation of a plane or circular wavefront and diffraction of light which encounters a converging lens.

$$\sigma = 2.44\,\lambda/d \tag{11}$$

where λ is the wavelength of light and d is the linear diameter of the aperture.

Some reminders: Principle of Huygens-Fresnel

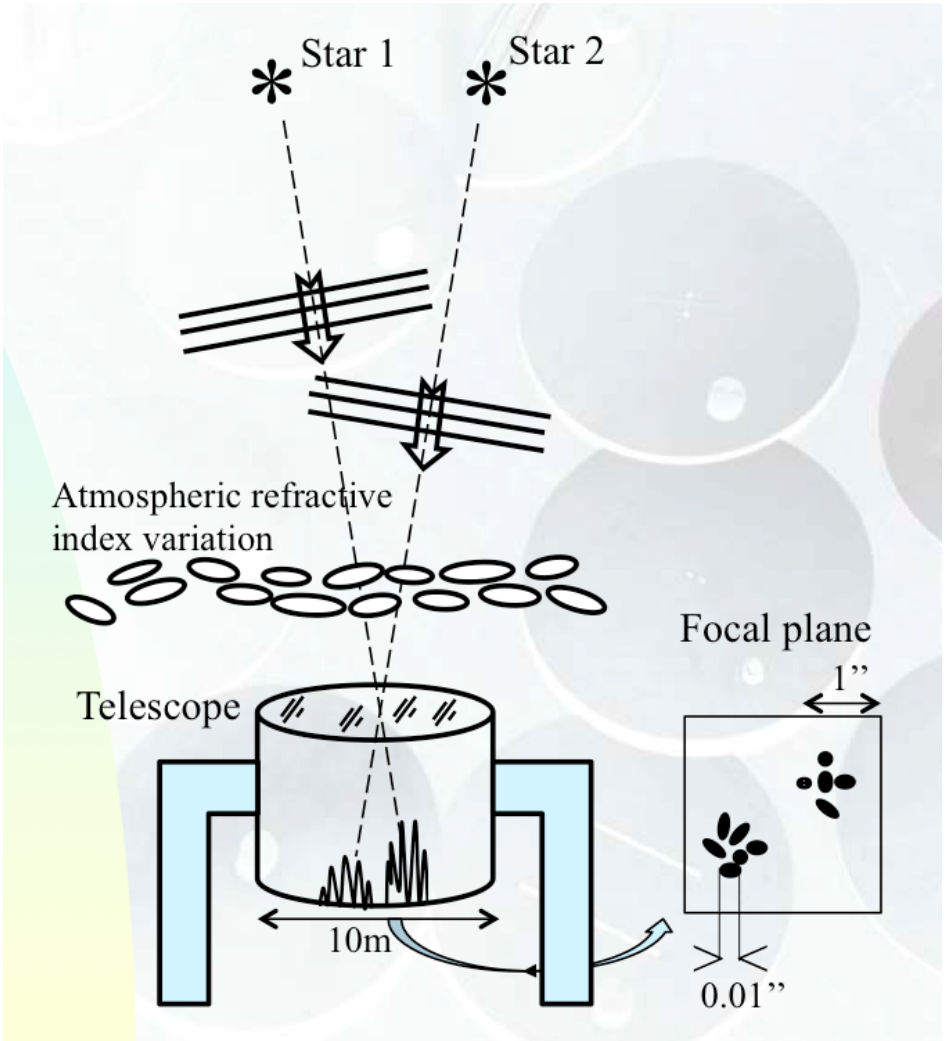

Figure: Atmospheric agitation above the objective of a large telescope causing the seeing effects seen in its focal plane.

Table of Contents

LIÈGE université

Brief history about the measurements of stellar diameters: Galileo

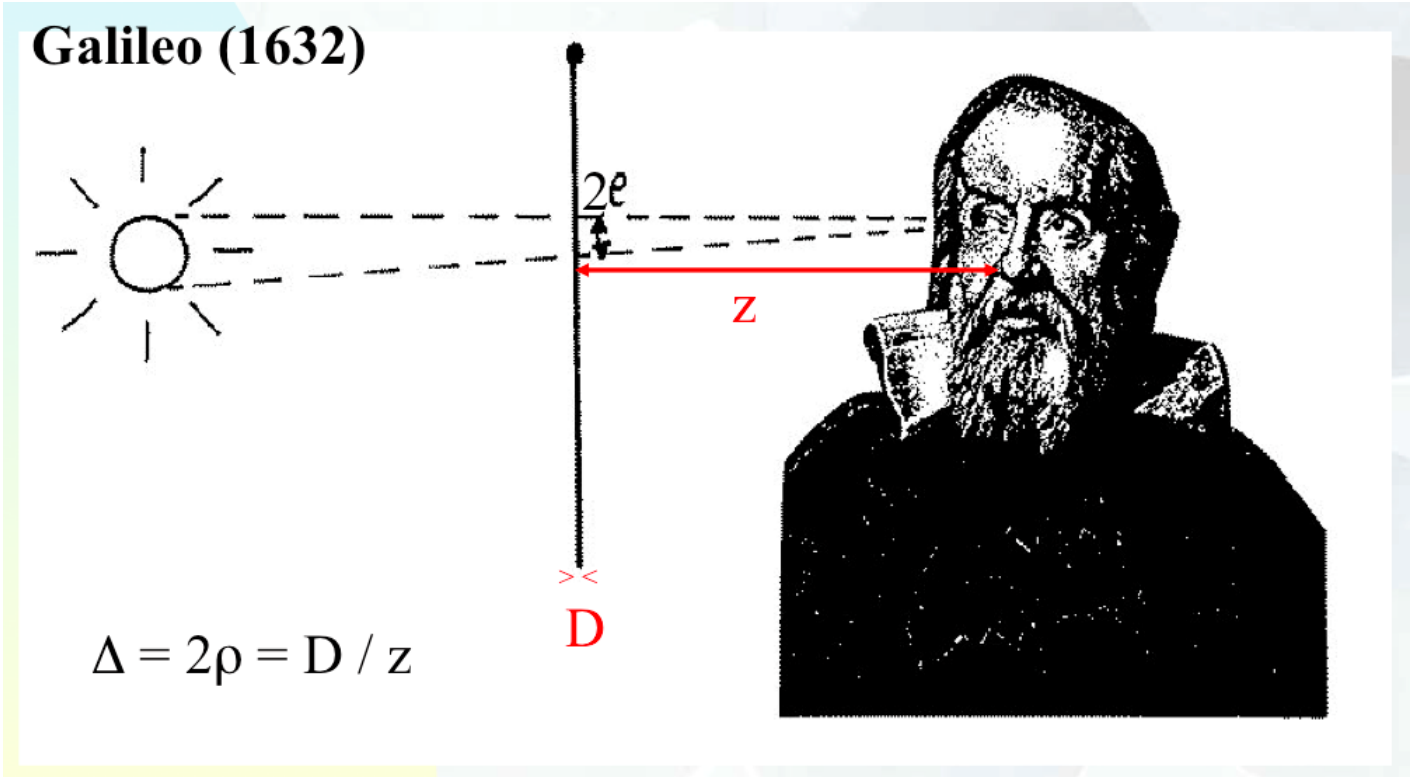

Figure: Experimental measurement by Galileo of the angular diameter of a star (see text).

Brief history about the measurements of stellar diameters: Newton

The angular diameter Δ of the Sun should be of the order of $2\,10^{-3}$" (with the current value of the visual apparent magnitude of the Sun, $V_\odot$ = -26.7, we find $\sim 8\,10^{-3}$"). It should be noted that the value currently established for the star Vega with modern interferometers is $3\,10^{-3}$". The formula to be used to establish this result can be obtained as follows: the angular diameter of the Sun Δ placed at the distance of Vega ($V = 0$) is given by the product of the apparent angular diameter of the Sun $\Delta_\odot$ times the factor $10^{V_\odot/5}$. As a reminder, the apparent diameter of the Sun is about 30'.

Brief history about the measurements of stellar diameters: Fizeau-type interferometry

Let us first remind the results obtained in the Young double hole experiment (1803, see Fig. 13).

Brief history about the measurements of stellar diameters: Fizeau-type interferometry

Let us first remind the results obtained in the Young double hole experiment (1803, see Fig. 13).

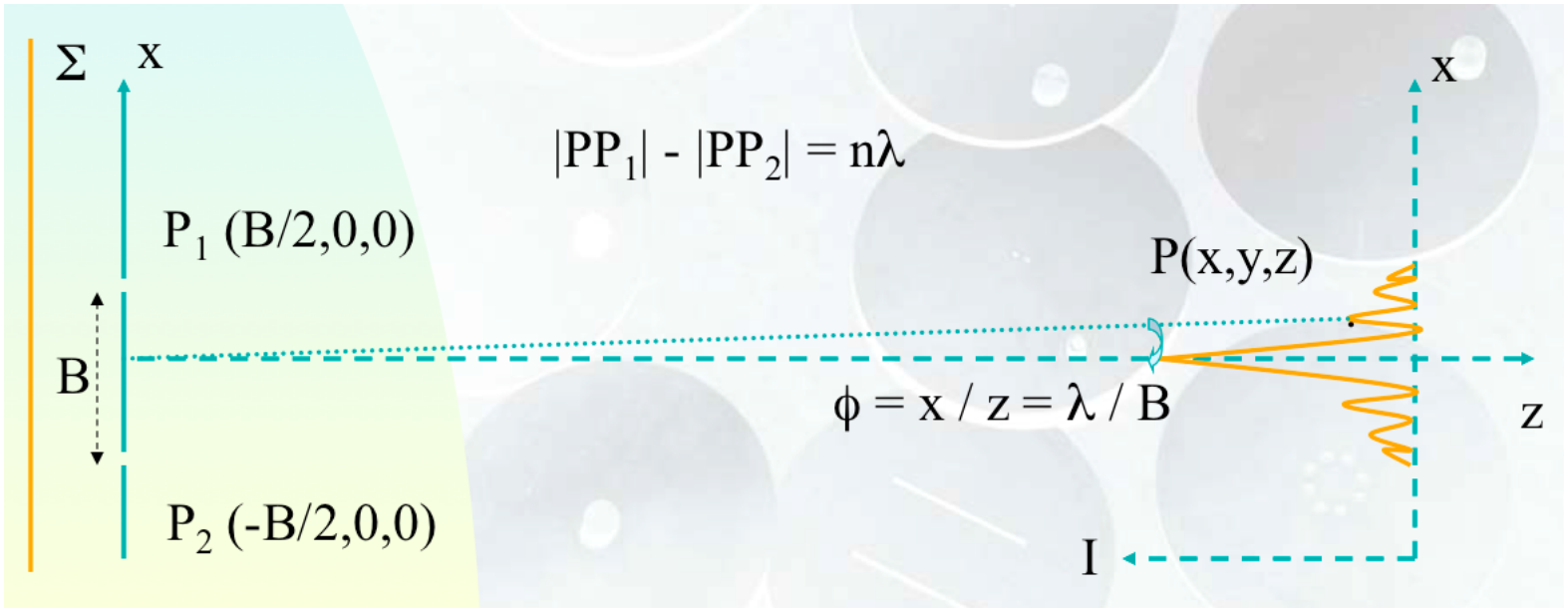

Figure: The double hole experiment of Young (see text).

Brief history about the measurements of stellar diameters: Fizeau-type interferometry

The locus of points $P(x, y, z)$ with cartesian coordinates x, y, z (see Fig. 13) where there will be a constructive interference is thus given by

$$|P_1P| - |P_2P| = n\lambda \tag{12}$$

with $n = 0, \pm 1, \pm 2$, etc.

The locus of points $P(x, y, z)$ with cartesian coordinates x, y, z (see Fig. 13) where there will be a constructive interference is thus given by

$$|P_1P| - |P_2P| = n\lambda \tag{12}$$

with $n = 0, \pm 1, \pm 2$, etc.
Let the points $P_i(x_i, y_i, 0)$ in the screen plane and $P(x, y, z)$ in the observer plane be such that $|x_i|, |y_i|, |x|, |y| << |z|$. We then find that

$$|P_iP| = \{(x - x_i)^2 + (y - y_i)^2 + z^2\}^{1/2} \tag{13}$$

The locus of points $P(x, y, z)$ with cartesian coordinates x, y, z (see Fig. 13) where there will be a constructive interference is thus given by

$$|P_1P| - |P_2P| = n\lambda \tag{12}$$

with $n = 0, \pm 1, \pm 2$, etc.
Let the points $P_i(x_i, y_i, 0)$ in the screen plane and $P(x, y, z)$ in the observer plane be such that $|x_i|, |y_i|, |x|, |y| << |z|$. We then find that

$$|P_iP| = \{(x - x_i)^2 + (y - y_i)^2 + z^2\}^{1/2} \tag{13}$$

which can be simplified at first order (given the above conditions) as follows:

$$|P_iP| = z\{1 + \frac{(x - x_i)^2 + (y - y_i)^2}{2z^2}\}. \tag{14}$$

Considering the two points P_1 and P_2 in the Young's screen, Eq. (12) reduces to

$$z\{1+\frac{(x+B/2)^2+y^2)}{2z^2}\}-z\{1+\frac{(x-B/2)^2+y^2}{2z^2}\}=n\lambda \tag{15}$$

Considering the two points P_1 and P_2 in the Young's screen, Eq. (12) reduces to

$$z\{1+\frac{(x+B/2)^2+y^2)}{2z^2}\}-z\{1+\frac{(x-B/2)^2+y^2}{2z^2}\}=n\lambda \tag{15}$$

and finally

$$\frac{xB}{z}=n\lambda \tag{16}$$

Considering the two points P_1 and P_2 in the Young's screen, Eq. (12) reduces to

$$z\{1+\frac{(x+B/2)^2+y^2)}{2z^2}\}-z\{1+\frac{(x-B/2)^2+y^2}{2z^2}\}=n\lambda \tag{15}$$

and finally

$$\frac{xB}{z}=n\lambda \tag{16}$$

or else

$$\Phi=\frac{x}{z}=n\frac{\lambda}{B}. \tag{17}$$

Brief history about the measurements of stellar diameters: Fizeau-type interferometry

If $\Delta \geq \phi/2 = \lambda / (2B)$,

fringe disappearance!

Fringe visibility:

$$v = \left(\frac{I_{max} - I_{min}}{I_{max} + I_{min}} \right)$$

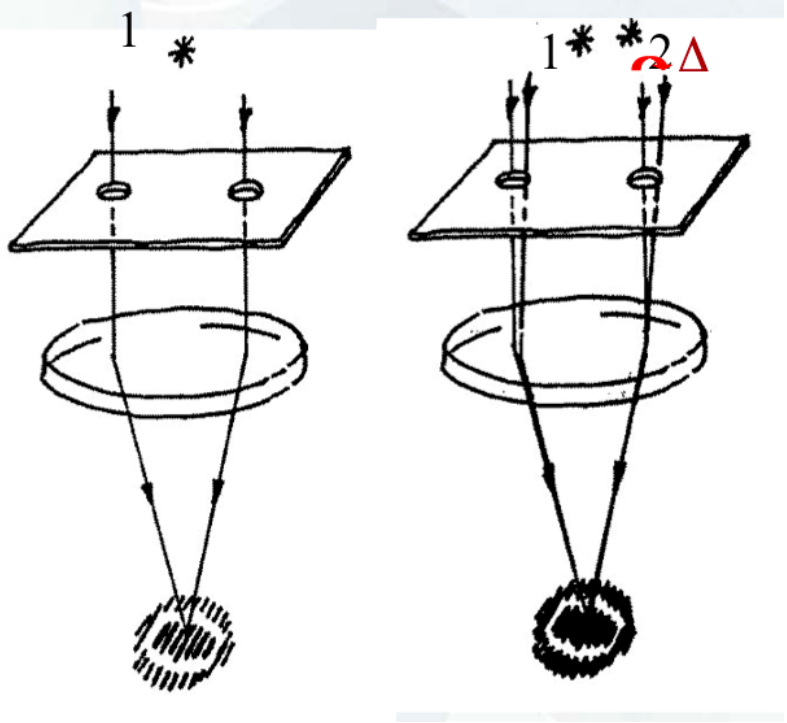

Figure: Fizeau, the father of stellar interferometry (1868; see text).

Brief history about the measurements of stellar diameters: Fizeau-type interferometry

If $\Delta \geq \phi/2 = \lambda / (2B)$,

fringe disappearance!

Fringe visibility:

$$v = \left(\frac{I_{max} - I_{min}}{I_{max} + I_{min}} \right)$$

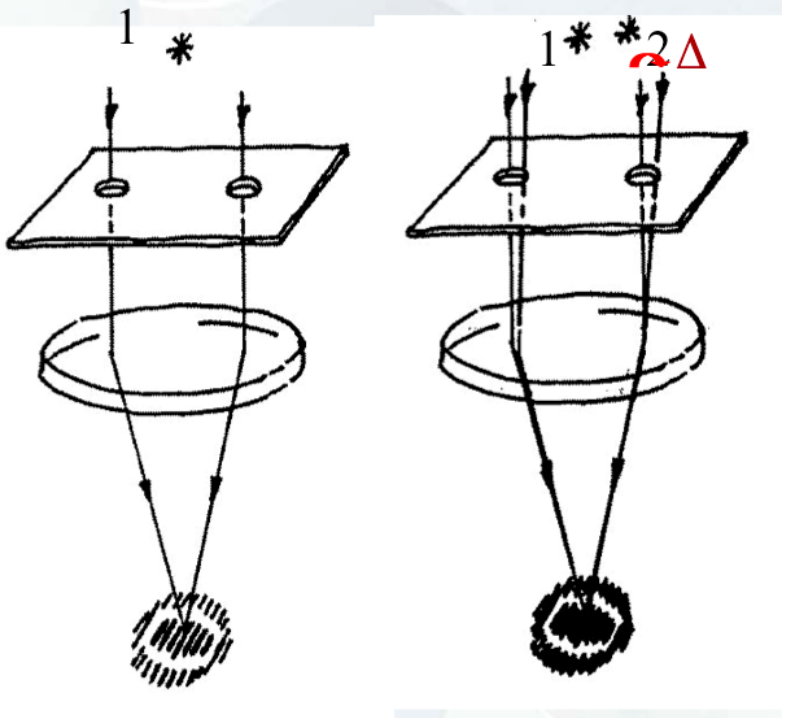

Figure: Fizeau, the father of stellar interferometry (1868; see text).

From Fig. 14, it is clear that the visibility of the fringes will significantly decrease whenever the following condition takes place

$$\Delta > \frac{\Phi}{2} = \frac{\lambda}{2B}. \quad (18)$$

Brief history about the measurements of stellar diameters: Fizeau-type interferometry

A quantity that objectively measures the contrast of the fringes is called the visibility.

Brief history about the measurements of stellar diameters: Fizeau-type interferometry

A quantity that objectively measures the contrast of the fringes is called the visibility. It is defined by the following expression:

$$v = \left(\frac{I_{\max} - I_{\min}}{I_{\max} + I_{\min}} \right). \tag{19}$$

Brief history about the measurements of stellar diameters: Fizeau-type interferometry

A quantity that objectively measures the contrast of the fringes is called the visibility. It is defined by the following expression:

$$v = \left(\frac{I_{\max} - I_{\min}}{I_{\max} + I_{\min}} \right). \tag{19}$$

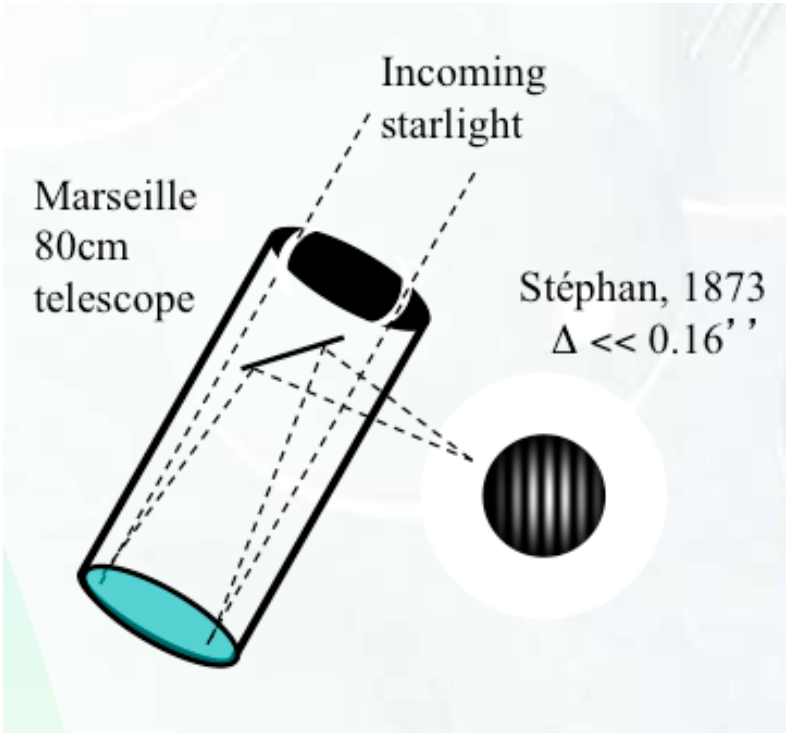

Figure: Diagram illustrating the way Fizeau and Stephan proceeded in order to measure the angular diameters of stars with the interferometric technique.

Brief history about the measurements of stellar diameters: Fizeau-type interferometry

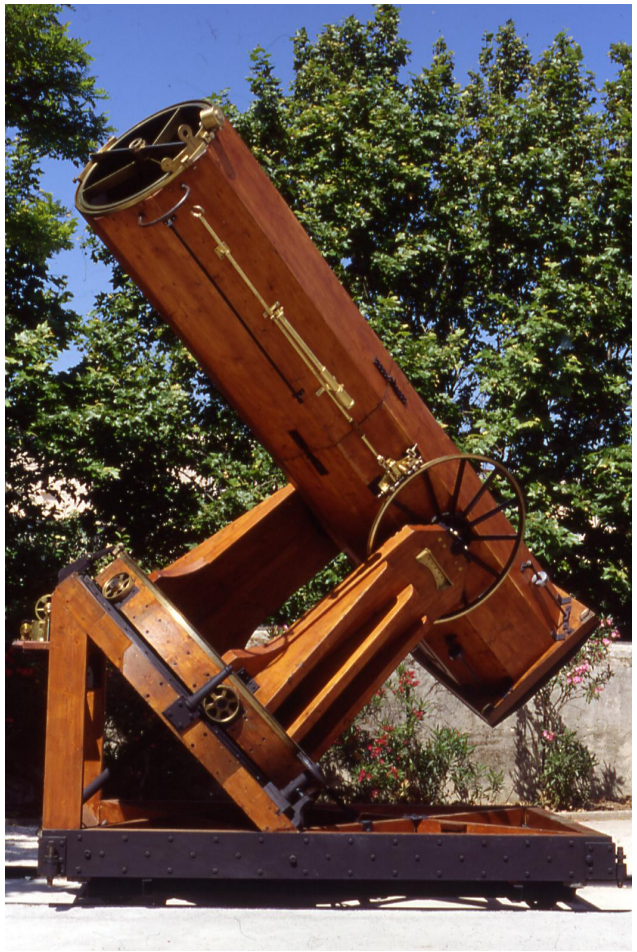

Figure: The 80cm Marseille telescope used by Fizeau and Stephan. © Michel Marcelin.

Brief history about the measurements of stellar diameters: Fizeau-type interferometry

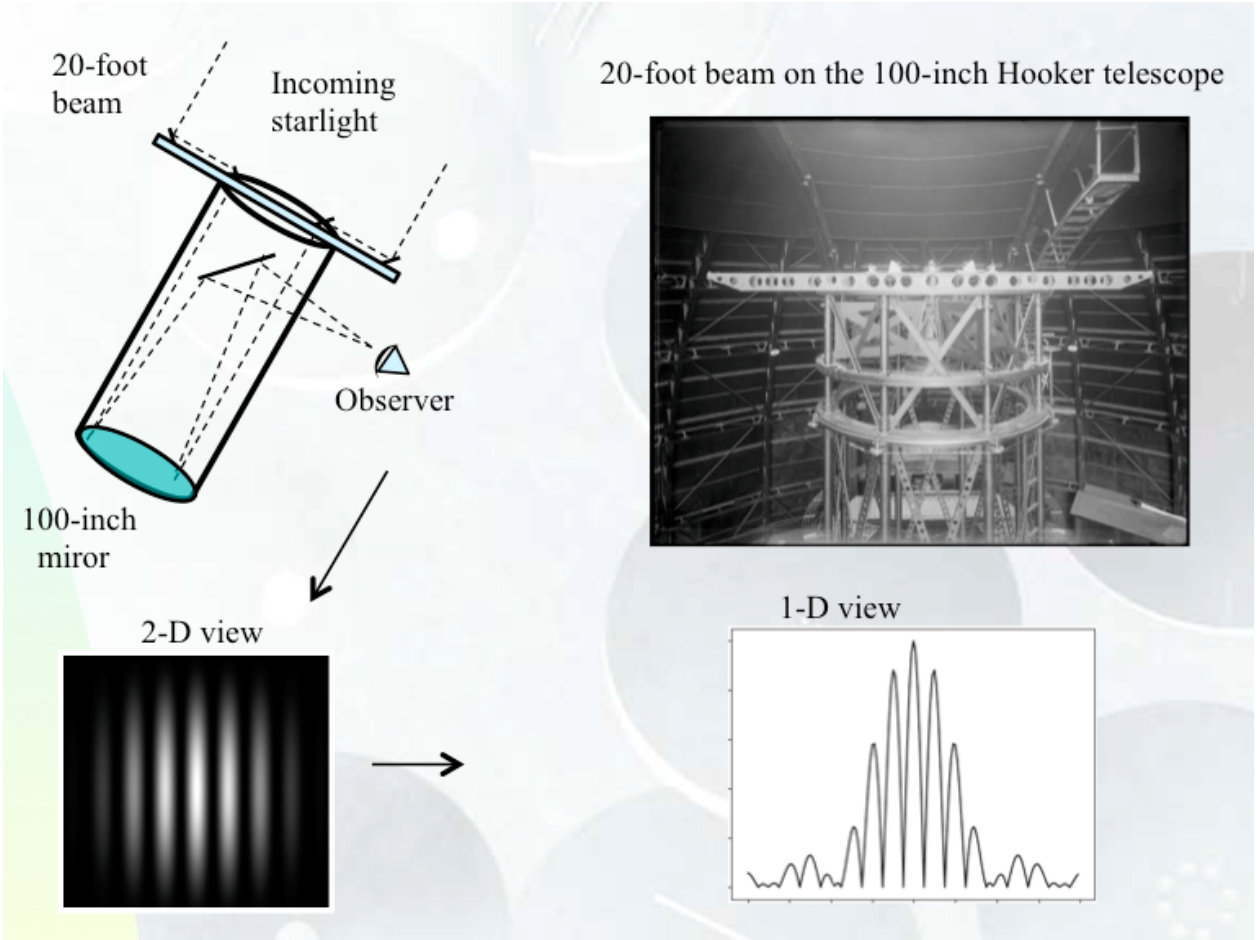

Figure: The stellar interferometer of Michelson-Pease set on top of the 2.5m Mount Wilson telescope. © The Observatories of the Carnegie Institution.

Different possible recombination schemes

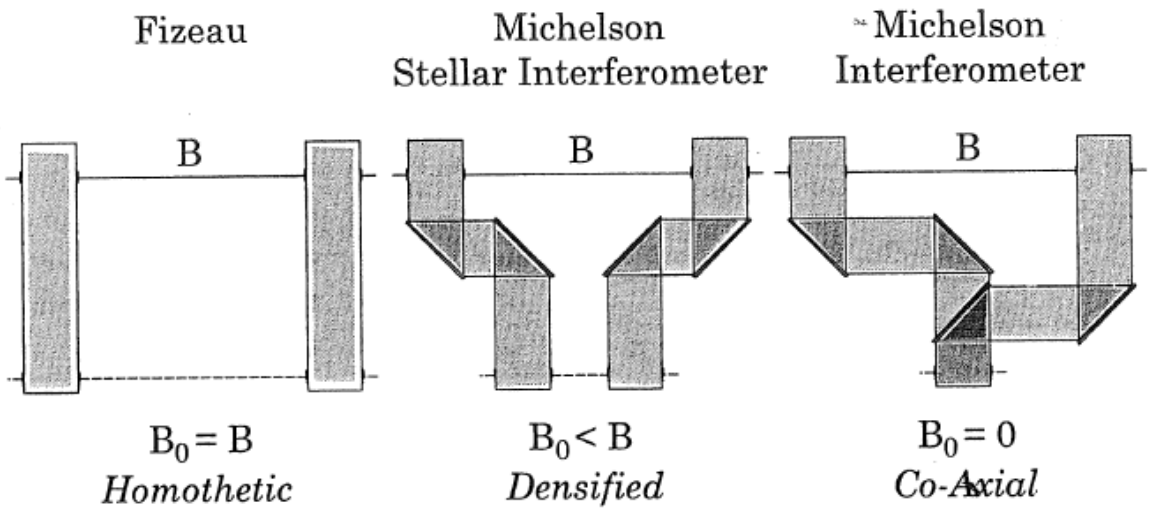

Figure: This illustration represents different possibilities for exit pupil placement, for a general exit baseline B_0.

Brief history about the measurements of stellar diameters: Fizeau-type interferometry

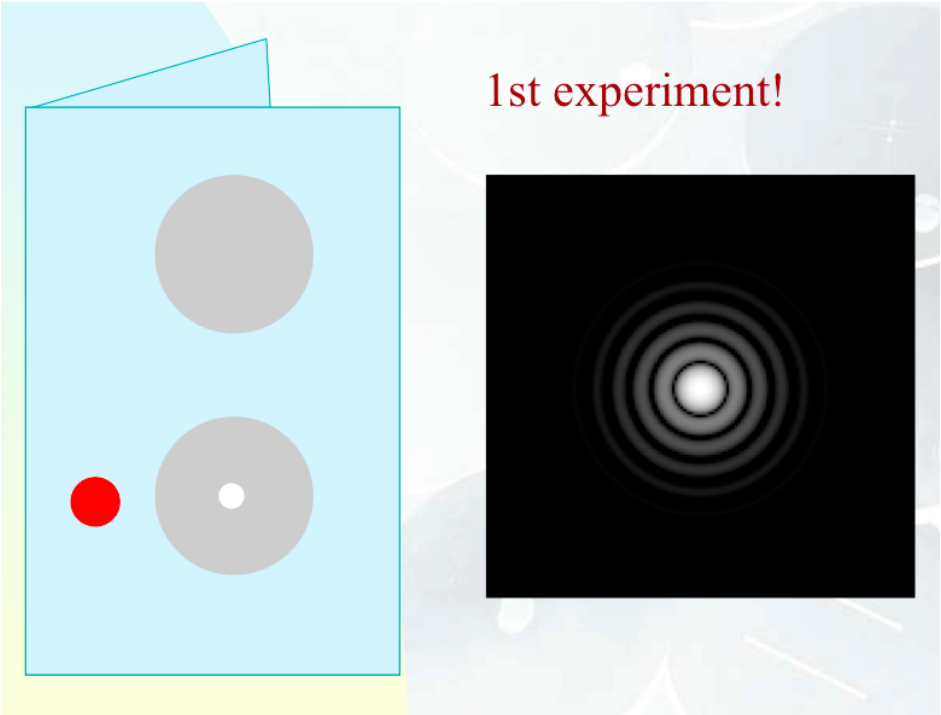

Figure: The one hole screen experiment: the small circular hole drilled in the aluminium paper is visible inside the lower bigger hole perforated in the cartoon screen. When looking through this hole at a distant light bulb, you perceive a nice Airy disk (cf. right image).

Brief history about the measurements of stellar diameters: Fizeau-type interferometry

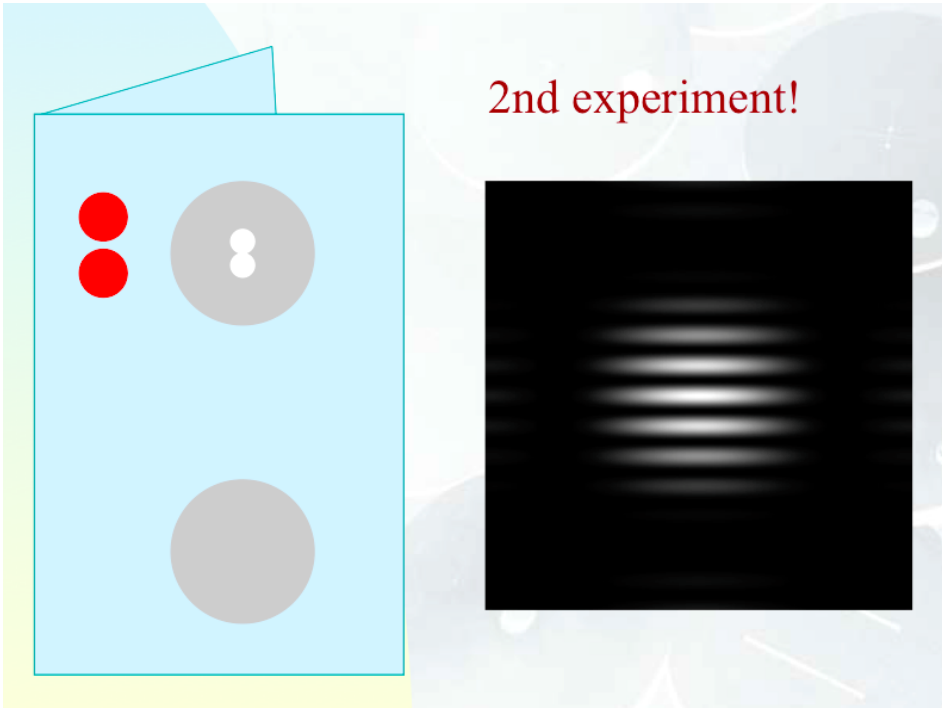

Figure: The two hole screen experiment: the two small circular holes drilled in the aluminium paper are visible inside the upper bigger hole perforated in the cartoon screen. When looking through these two holes at a distant light bulb, you perceive a nice Airy disk superimposed by a pattern of bright and dark fringes (cf. right image).

Table of Contents

Light coherence: quasi-monochromatic light

This theory consists essentially in a statistical description of the properties of the radiation field in terms of the correlation between electromagnetic vibrations at different points in the field.

Light coherence: quasi-monochromatic light

This theory consists essentially in a statistical description of the properties of the radiation field in terms of the correlation between electromagnetic vibrations at different points in the field.
The light emitted by a real source (see Fig. 21) is of course not monochromatic. As in the case of a monochromatic wave, the intensity of such a radiation field at any point in space is defined by

$$I = \langle V(t)V(t)^* \rangle . \tag{20}$$

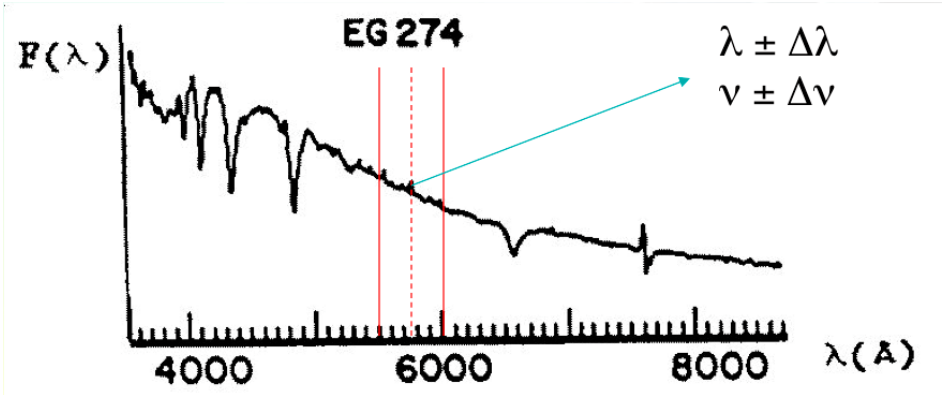

Figure: Stars do not emit monochromatic light. Quasi monochromatic light is assumed to be emitted at the wavelength λ (resp. the frequency ν) within the bandwidth $\pm\Delta\lambda$ (resp. $\pm\Delta\nu$).

Light coherence: quasi-monochromatic light

In order to determine the electric field created by such a source, emitting within a certain frequency range $\pm\Delta\nu$, we must sum up the fields due to all the individual monochromatic components such that the resulting electric field $V(z,t)$ is given by the real part of the following expression:

$$V(z,t) = \int_{\nu-\Delta\nu}^{\nu+\Delta\nu} a(\nu') \exp[i2\pi(\nu' t - z/\lambda')] d\nu'. \tag{21}$$

Light coherence: quasi-monochromatic light

In order to determine the electric field created by such a source, emitting within a certain frequency range $\pm\Delta\nu$, we must sum up the fields due to all the individual monochromatic components such that the resulting electric field $V(z,t)$ is given by the real part of the following expression:

$$V(z,t) = \int_{\nu-\Delta\nu}^{\nu+\Delta\nu} a(\nu') \exp[i2\pi(\nu' t - z/\lambda')] d\nu'. \tag{21}$$

While a monochromatic beam of radiation corresponds to an infinitely long wave train, it can easily be shown that the superposition of multiple infinitely long wave trains, with nearly similar frequencies, results in the formation of wave groups.

In order to determine the electric field created by such a source, emitting within a certain frequency range $\pm\Delta\nu$, we must sum up the fields due to all the individual monochromatic components such that the resulting electric field $V(z,t)$ is given by the real part of the following expression:

$$V(z,t) = \int_{\nu-\Delta\nu}^{\nu+\Delta\nu} a(\nu') \exp[i2\pi(\nu' t - z/\lambda')] d\nu'. \tag{21}$$

While a monochromatic beam of radiation corresponds to an infinitely long wave train, it can easily be shown that the superposition of multiple infinitely long wave trains, with nearly similar frequencies, results in the formation of wave groups.
Indeed, we find that Eq. (21) may be rewritten as

$$V(z,t) = A(z,t) \exp[i2\pi(\nu t - z/\lambda)] \tag{22}$$

where

$$A(z,t) = \int_{\nu-\Delta\nu}^{\nu+\Delta\nu} a(\nu') \exp\{i2\pi[(\nu'-\nu)t - z(1/\lambda' - 1/\lambda)]\} d\nu'. \tag{23}$$

Light coherence: quasi-monochromatic light

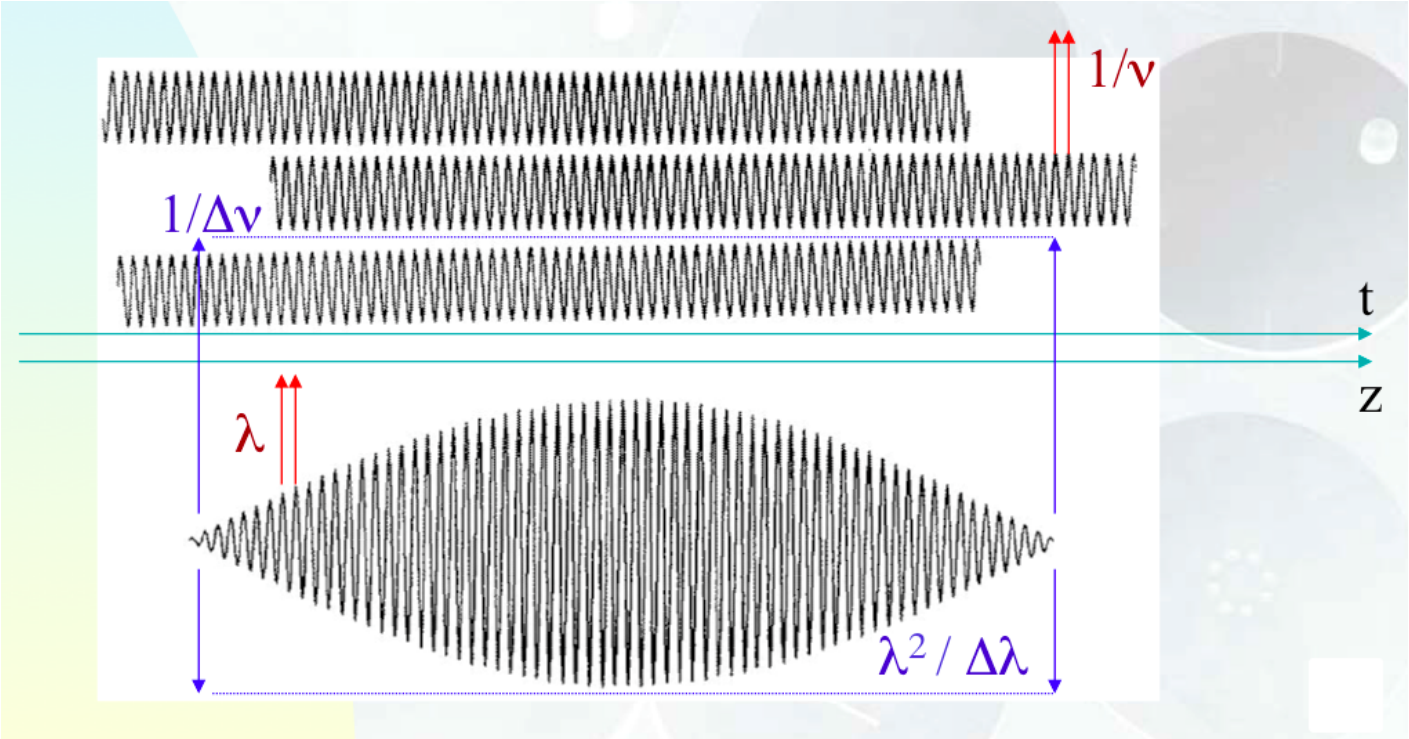

Figure: Superposition of long wave trains having quite similar frequencies ν' in the range $\nu \pm \Delta\nu$ (resp. wavelengths λ' in the range $\lambda \pm \Delta\lambda$) results in the propagation of a long wave train with the frequency ν (resp. wavelength λ) but which amplitude $A(z,t)$ is varying with a lower frequency $\Delta\nu$ (resp. longer wavelength $\lambda^2/\Delta\lambda$).

Light coherence: visibility of the interference fringes

What becomes the visibility of the interference fringes in the Young's hole experiment for the case of a quasi-monochromatic source having a finite dimension?

Light coherence: visibility of the interference fringes

What becomes the visibility of the interference fringes in the Young's hole experiment for the case of a quasi-monochromatic source having a finite dimension?

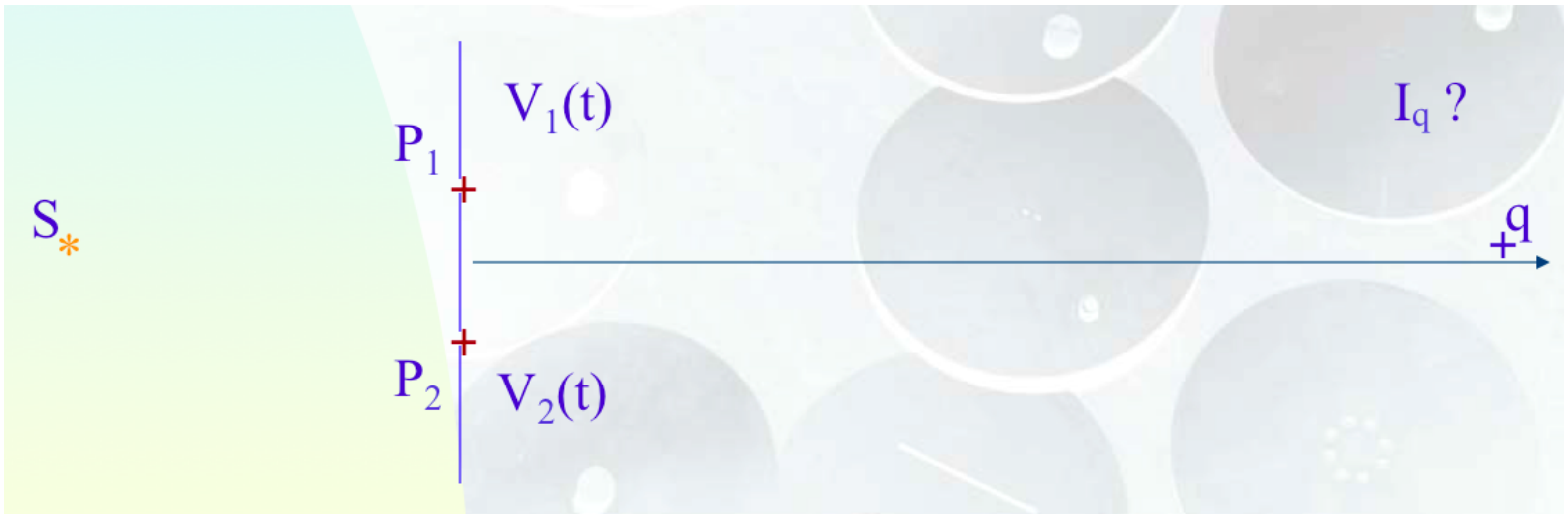

Figure: Assuming an extended source S which quasi monochromatic light passes through the two holes P_1 and P_2, I_q represents the intensity distribution at the point q which accounts for the formation of the interference fringes.

We can re-write the expression of the intensity I_q at point q as indicated below (see Eqs. (24)-(27)). It is assumed that the holes placed at the points P_1, P_2 in the Young plane have the same aperture size (i.e. $V_1(t) = V_2(t)$) and that the propagation times of the light between P_1 (resp. P_2) and q are t_{1q} (resp. t_{2q}, see Fig. 23) :

$$I_q = \left\langle V_q^*(t) V_q(t) \right\rangle , \tag{24}$$

Light coherence: visibility of the interference fringes

We can re-write the expression of the intensity I_q at point q as indicated below (see Eqs. (24)-(27)). It is assumed that the holes placed at the points P_1, P_2 in the Young plane have the same aperture size (i.e. $V_1(t) = V_2(t)$) and that the propagation times of the light between P_1 (resp. P_2) and q are t_{1q} (resp. t_{2q}, see Fig. 23) :

$$I_q = \left\langle V_q^*(t) V_q(t) \right\rangle, \tag{24}$$

$$V_q(t) = V_1(t - t_{1q}) + V_2(t - t_{2q}) \tag{25}$$

Light coherence: visibility of the interference fringes

We can re-write the expression of the intensity I_q at point q as indicated below (see Eqs. (24)-(27)). It is assumed that the holes placed at the points P_1, P_2 in the Young plane have the same aperture size (i.e. $V_1(t) = V_2(t)$) and that the propagation times of the light between P_1 (resp. P_2) and q are t_{1q} (resp. t_{2q}, see Fig. 23) :

$$I_q = \left\langle V_q^*(t) V_q(t) \right\rangle , \tag{24}$$

$$V_q(t) = V_1(t - t_{1q}) + V_2(t - t_{2q}) \tag{25}$$

and after a mere change of the time origin

$$V_q(t) = V_1(t) + V_2(t - \tau) \tag{26}$$

where we have defined

$$\tau = t_{2q} - t_{1q}. \tag{27}$$

Light coherence: visibility of the interference fringes

It follows that Eq. (24) can be easily transformed into (28) where (29) represents the complex degree of mutual coherence, and the intensity $I = < V_1 V_1^* > = < V_2 V_2^* >$.

$$I_q = I + I + 2I\,Re[\gamma_{12}(\tau)], \tag{28}$$

$$\gamma_{12}(\tau) = \langle V_1^*(t) V_2(t-\tau) \rangle / I. \tag{29}$$

It follows that Eq. (24) can be easily transformed into (28) where (29) represents the complex degree of mutual coherence, and the intensity $I =< V_1 V_1^* >=< V_2 V_2^* >$.

$$I_q = I + I + 2I\,Re[\gamma_{12}(\tau)], \tag{28}$$

$$\gamma_{12}(\tau) = \langle V_1^*(t) V_2(t-\tau)\rangle / I. \tag{29}$$

By means of (22), this function $\gamma_{12}(\tau)$ can still be expressed as (30), and if $\tau << 1/\Delta\nu$ (i.e. the difference between the arrival times of the two light rays is less than the beat period $1/\Delta\nu$), we can give it the form (31):

$$\gamma_{12}(\tau) = \langle A_1^*(z,t) A_2(z,t-\tau)\rangle \exp(-i2\pi\nu\tau)/I, \tag{30}$$

and if $\tau << 1/\Delta\nu$

$$\gamma_{12}(\tau) = |\gamma_{12}(\tau=0)| \exp(i\beta_{12} - i2\pi\nu\tau). \tag{31}$$

Light coherence: visibility of the interference fringes

Equation (28) can then be rewritten as (32) and in this case the visibility v of the interference fringes is $|\gamma_{12}(\tau = 0)|$ (see Eq. (33)), I_{max} and I_{min} representing the brightest and weakest fringe intensities.

$$I_q = I + I + 2I\,|\gamma_{12}(\tau = 0)|\,cos(\beta_{12} - 2\pi\nu\tau) \tag{32}$$

Equation (28) can then be rewritten as (32) and in this case the visibility v of the interference fringes is $|\gamma_{12}(\tau = 0)|$ (see Eq. (33)), I_{max} and I_{min} representing the brightest and weakest fringe intensities.

$$I_q = I + I + 2I\,|\gamma_{12}(\tau = 0)|\,cos(\beta_{12} - 2\pi\nu\tau) \tag{32}$$

and

$$v = \left(\frac{I_{\text{max}} - I_{\text{min}}}{I_{\text{max}} + I_{\text{min}}}\right) = |\gamma_{12}(\tau = 0)|. \tag{33}$$

Light coherence: visibility of the interference fringes

We propose hereafter to the reader to answer the two following questions:

Light coherence: visibility of the interference fringes

We propose hereafter to the reader to answer the two following questions:

What is the value of $|\gamma_{12}(\tau = 0)|$ in the Young's holes experiment for the case of a monochromatic wave, two point-like holes and an infinitely small point-like source?

Light coherence: visibility of the interference fringes

We propose hereafter to the reader to answer the two following questions:

What is the value of $|\gamma_{12}(\tau = 0)|$ in the Young's holes experiment for the case of a monochromatic wave, two point-like holes and an infinitely small point-like source?

And what can we say about the source when $|\gamma_{12}(\tau = 0)| = 0$?

Light coherence: visibility of the interference fringes

We propose hereafter to the reader to answer the two following questions:

What is the value of $|\gamma_{12}(\tau = 0)|$ in the Young's holes experiment for the case of a monochromatic wave, two point-like holes and an infinitely small point-like source?

And what can we say about the source when $|\gamma_{12}(\tau = 0)| = 0$?

Light coherence: visibility of the interference fringes

We propose hereafter to the reader to answer the two following questions:

What is the value of $|\gamma_{12}(\tau = 0)|$ in the Young's holes experiment for the case of a monochromatic wave, two point-like holes and an infinitely small point-like source?

And what can we say about the source when $|\gamma_{12}(\tau = 0)| = 0$?

In the lecture notes that will become available to you thanks to Jaime Alonso, you will see that the module of $\gamma_{12}(\tau = 0)$ is directly related to the structure of the source that we are observing. It directly comes from the demonstration of the Zernicke-van Cittert theorem which is too long to present here to-day.

LIÈGE université

Apart from a multiplicative factor, we demonstrate in the lecture notes that the visibility of the fringes (the function $|\gamma_{12}(\tau = 0)|$) is simply the modulus of the Fourier transform of the normalized surface brightness I' of the source (Eq. (35)).

$$\gamma_{12}(0, X/\lambda, Y/\lambda) = \exp(-i\phi_{X,Y}) \int\int_S I'(\zeta, \eta) \exp[-i2\pi(X\zeta + Y\eta)/\lambda] d\zeta d\eta \qquad (34)$$

with

$$I'(\zeta, \eta) = \frac{I(\zeta, \eta)}{\int\int_S I(\zeta', \eta') d\zeta' d\eta'}. \qquad (35)$$

Light coherence: Zernicke-vanCittert theorem

Apart from a multiplicative factor, we demonstrate in the lecture notes that the visibility of the fringes (the function $|\gamma_{12}(\tau = 0)|$) is simply the modulus of the Fourier transform of the normalized surface brightness I' of the source (Eq. (35)).

$$\gamma_{12}(0, X/\lambda, Y/\lambda) = \exp(-i\phi_{X,Y}) \int\int_S I'(\zeta, \eta) \exp[-i2\pi(X\zeta + Y\eta)/\lambda] d\zeta d\eta \qquad (34)$$

with

$$I'(\zeta, \eta) = \frac{I(\zeta, \eta)}{\int\int_S I(\zeta', \eta') d\zeta' d\eta'}. \qquad (35)$$

Defining the angular space frequencies $u = X/\lambda$, $v = Y/\lambda$, Eq. (34) becomes

$$\gamma_{12}(0,u,v) = \exp(-i\phi_{u,v}) \int\int_S I'(\zeta,\eta)\, \exp[-i2\pi(u\zeta + v\eta)] d\zeta d\eta. \quad (36)$$

$$\gamma_{12}(0,u,v) = \exp(-i\phi_{u,v}) \int\int_S I'(\zeta,\eta)\, \exp[-i2\pi(u\zeta + v\eta)] d\zeta d\eta. \quad (36)$$

By a simple inverse Fourier transform, it is then possible to recover the surface (normalized) brightness of the source with an angular resolution equivalent to that of a telescope whose effective diameter would be equal to the baseline of the interferometer consisting of two independent telescopes

$$I'(\zeta,\eta) = \int\int \gamma_{12}(0,u,v)\, \exp(i\phi_{u,v})\, \exp[i2\pi(\zeta u + \eta v)] du dv. \quad (37)$$

$$\gamma_{12}(0,u,v) = \exp(-i\phi_{u,v}) \int\int_S I'(\zeta,\eta)\, \exp[-i2\pi(u\zeta + v\eta)] d\zeta d\eta. \quad (36)$$

By a simple inverse Fourier transform, it is then possible to recover the surface (normalized) brightness of the source with an angular resolution equivalent to that of a telescope whose effective diameter would be equal to the baseline of the interferometer consisting of two independent telescopes

$$I'(\zeta,\eta) = \int\int \gamma_{12}(0,u,v)\, \exp(i\phi_{u,v})\, \exp[i2\pi(\zeta u + \eta v)] du dv. \quad (37)$$

Equations (36) and (37) thus clearly highlight the power of the complex degree of mutual coherence since they make it possible to link the visibility and the normalized intensity distribution of the source by means of the Fourier transform $v = |\gamma_{12}(0)| = |TF_{-}(I')|$, and its inverse.

Light coherence: Zernicke-vanCittert theorem

$$\gamma_{12}(0,u,v) = \exp(-i\phi_{u,v}) \int\int_S I'(\zeta,\eta)\, \exp[-i2\pi(u\zeta + v\eta)] d\zeta d\eta. \quad (36)$$

By a simple inverse Fourier transform, it is then possible to recover the surface (normalized) brightness of the source with an angular resolution equivalent to that of a telescope whose effective diameter would be equal to the baseline of the interferometer consisting of two independent telescopes

$$I'(\zeta,\eta) = \int\int \gamma_{12}(0,u,v)\, \exp(i\phi_{u,v})\, \exp[i2\pi(\zeta u + \eta v)] du dv. \quad (37)$$

Equations (36) and (37) thus clearly highlight the power of the complex degree of mutual coherence since they make it possible to link the visibility and the normalized intensity distribution of the source by means of the Fourier transform $v = |\gamma_{12}(0)| = |TF_-(I')|$, and its inverse.
Aperture synthesis consists in observing a maximum number of visibilities of the source, thus trying to cover as well as possible the (u,v) plane from which we shall try, sometimes with some additional assumptions, to determine the structure of the source from the inverse Fourier transform (37) in which the integrant is not the visibility (i.e. the module of the complex degree of mutual coherence) but the complex degree of mutual coherence itself, within the factor $exp(i\phi_{x,y})$.

A nice application of the previous relation consists in deriving the visibility of a star which is seen as a projected $2-D$ uniform circular disk which angular radius is ρ_{UD} and its angular diameter θ_{UD}.

A nice application of the previous relation consists in deriving the visibility of a star which is seen as a projected $2-D$ uniform circular disk which angular radius is ρ_{UD} and its angular diameter θ_{UD}.

A nice application of the previous relation consists in deriving the visibility of a star which is seen as a projected $2-D$ uniform circular disk which angular radius is ρ_{UD} and its angular diameter θ_{UD}.

We would find that the expression (33) of the fringe visibility for the case of a star seen as a projected $2-D$ uniform circular disk with an angular dimater $\theta_{UD} = 2\rho_{UD}$ is

$$v = \left(\frac{I_{\max} - I_{\min}}{I_{\max} + I_{\min}}\right) = |\gamma_{12}(0,u)| = \left|\frac{2J_1(\pi\theta_{UD}u)}{\pi\theta_{UD}u}\right|, \tag{38}$$

where we have set $u = R/\lambda$.

As a reminder, the Bessel function has the following properties

$$J_1(x = 3.8317...) = 0$$
$$\lim_{x \to 0} \frac{J_1(x)}{x} = 1/2, \tag{39}$$

which allow us to easily understand the behavior of the visibility function illustrated in Fig. 24.

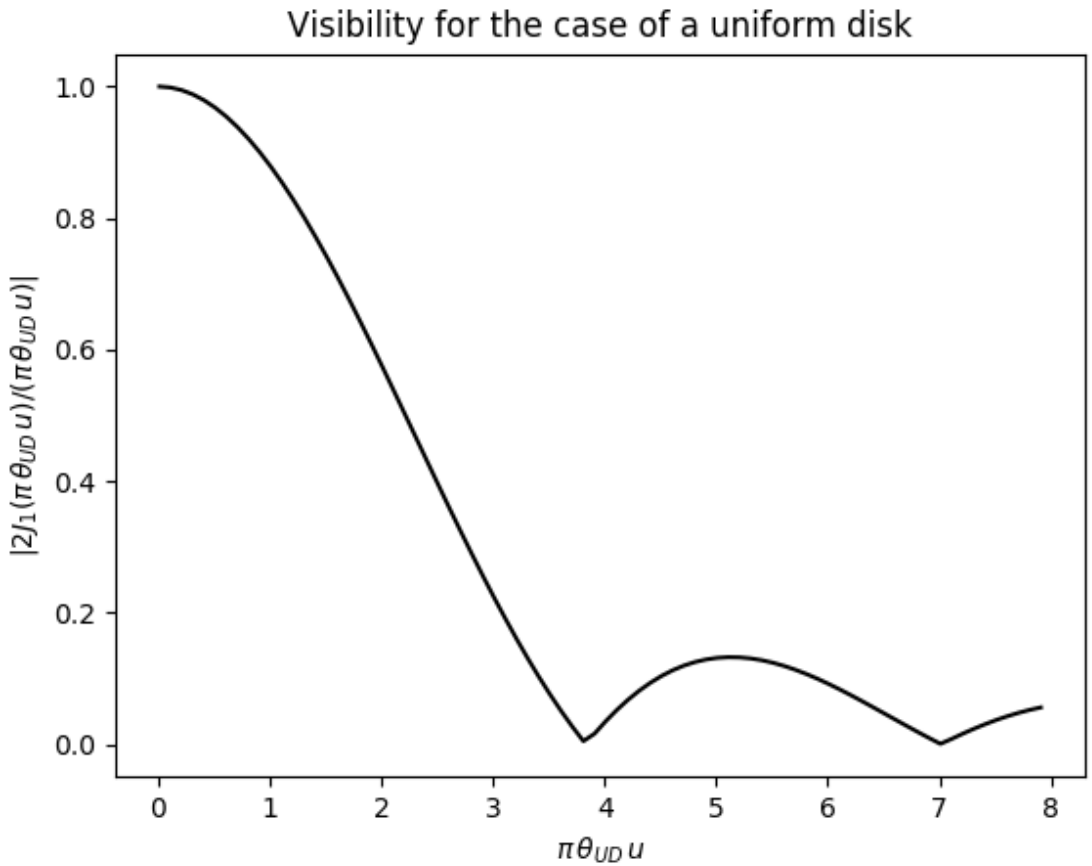

Figure: Visibility function expected for a star consisting of a uniformly bright circular disk with an angular diameter θ_{UD}.

One example of stellar visibilities

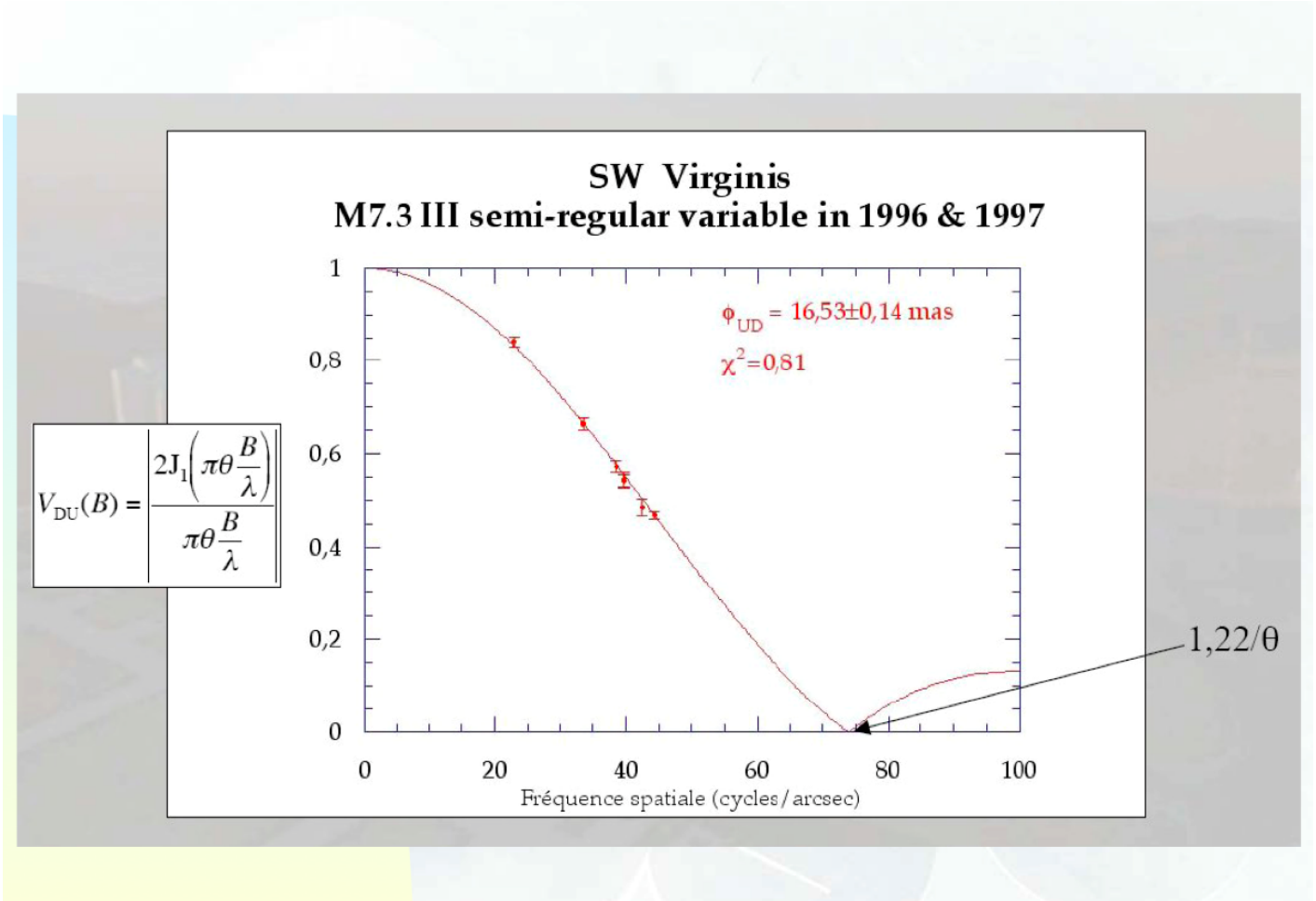

Figure: One example of stellar visibilities.

One could then wonder whether it is possible to observe interferometric fringes from our nearest star, i.e. the Sun?

Light coherence: some remarkable properties of the Fourier transform and applications

One could then wonder whether it is possible to observe interferometric fringes from our nearest star, i.e. the Sun? Figure 26 illustrates such fringes in while light obtained on 9th of April 2010 using a micro interferometer consisting of 2 holes with a diameter of 11.8 μ separated by a baseline of 29.4 μ. This micro-interferometer was placed in front of the objective of an EOS 5D Canon camera. Since the picture was taken in white light, it is possible to see the effects due to color dispersion. It is then easy to get an estimate of the fringe visibility, using Eq. (38), assuming that the Sun is a uniform disk with an angular diameter of 30'.

Figure: Solar fringes photographed with an EOS 5D Canon camera in front of which was set a micro-interferometer consisting of two holes having a diameter of 11.8μ separated by a baseline of 29.4μ.

Table of Contents

Some examples of interferometers

One of the most respected sanctuaries of optical interferometry is located on the plateau of Caussols, north of Grasse, in the south of France. The I2T (in French, "Interféromètre à 2 Télescopes"), made of 2 telescopes with an aperture of 26cm each and separated by a baseline of up to 144m was characterized by an angular resolution $\Phi \sim 0.001''$ attainable for objects with an apparent magnitude brighter than $V_{lim} \sim 6$ (see Figure 27, left).

Some examples of interferometers

One of the most respected sanctuaries of optical interferometry is located on the plateau of Caussols, north of Grasse, in the south of France. The I2T (in French, "Interféromètre à 2 Télescopes"), made of 2 telescopes with an aperture of 26cm each and separated by a baseline of up to 144m was characterized by an angular resolution $\Phi \sim 0.001''$ attainable for objects with an apparent magnitude brighter than $V_{lim} \sim 6$ (see Figure 27, left). First interference fringes were obtained on Vega in 1975 (Fig. 27, right).

Some examples of interferometers

One of the most respected sanctuaries of optical interferometry is located on the plateau of Caussols, north of Grasse, in the south of France. The I2T (in French, "Interféromètre à 2 Télescopes"), made of 2 telescopes with an aperture of 26cm each and separated by a baseline of up to 144m was characterized by an angular resolution $\Phi \sim 0.001''$ attainable for objects with an apparent magnitude brighter than $V_{lim} \sim 6$ (see Figure 27, left). First interference fringes were obtained on Vega in 1975 (Fig. 27, right). About twenty angular diameters of stars have been measured using the same I2T by Prof. Antoine Labeyrie and his close collaborators.

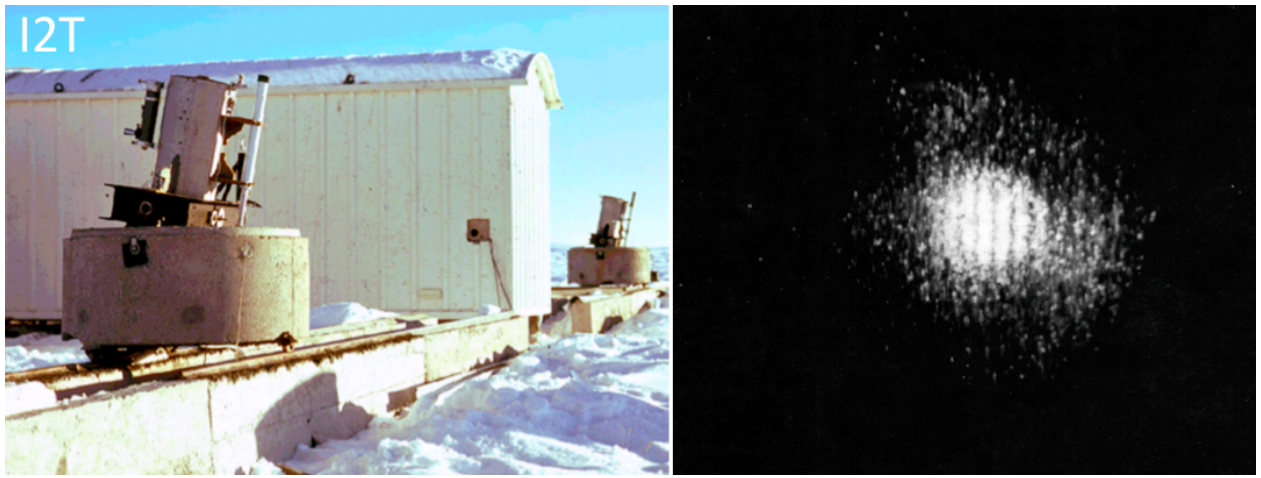

Figure: First fringes obtained with the I2T on Vega (Labeyrie et al. 1975, © Observatoire de la Côte d'Azur).

Some examples of interferometers

In order to equalize the light paths collected from the stars passing through the two telescopes, optical delay lines are mandatory. These have been successfully used for the first time in 1975 (see Fig. 28 for an illustration of how delay lines work).

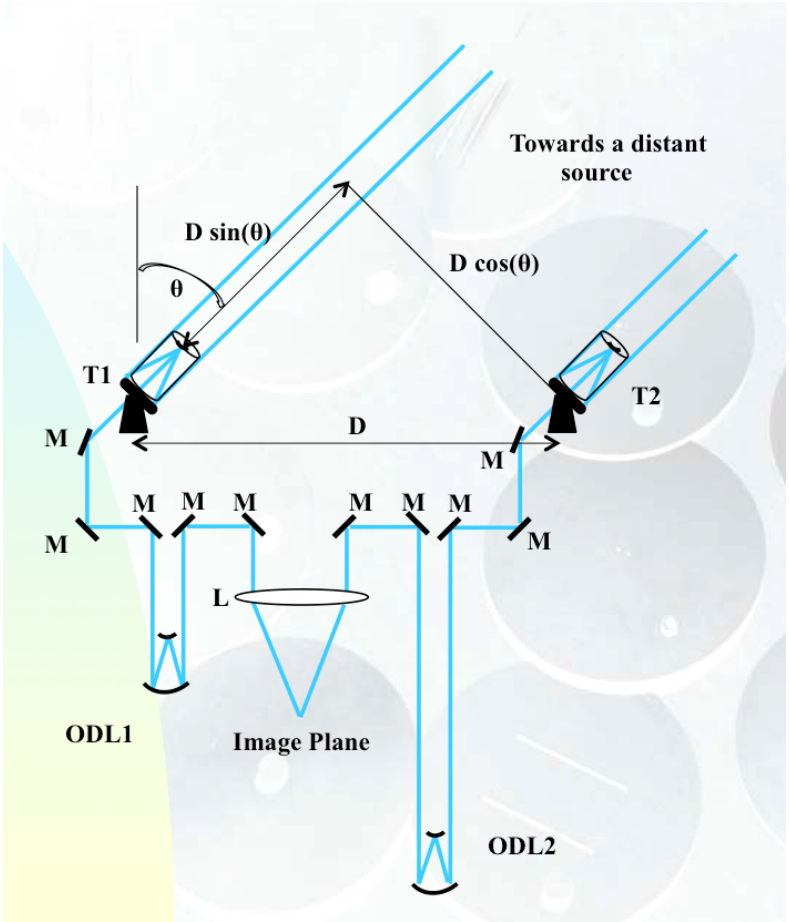

Figure: Use of optical delay lines to compensate for the continuous change in the lengths of the two light paths as the Earth rotates.

Some examples of interferometers

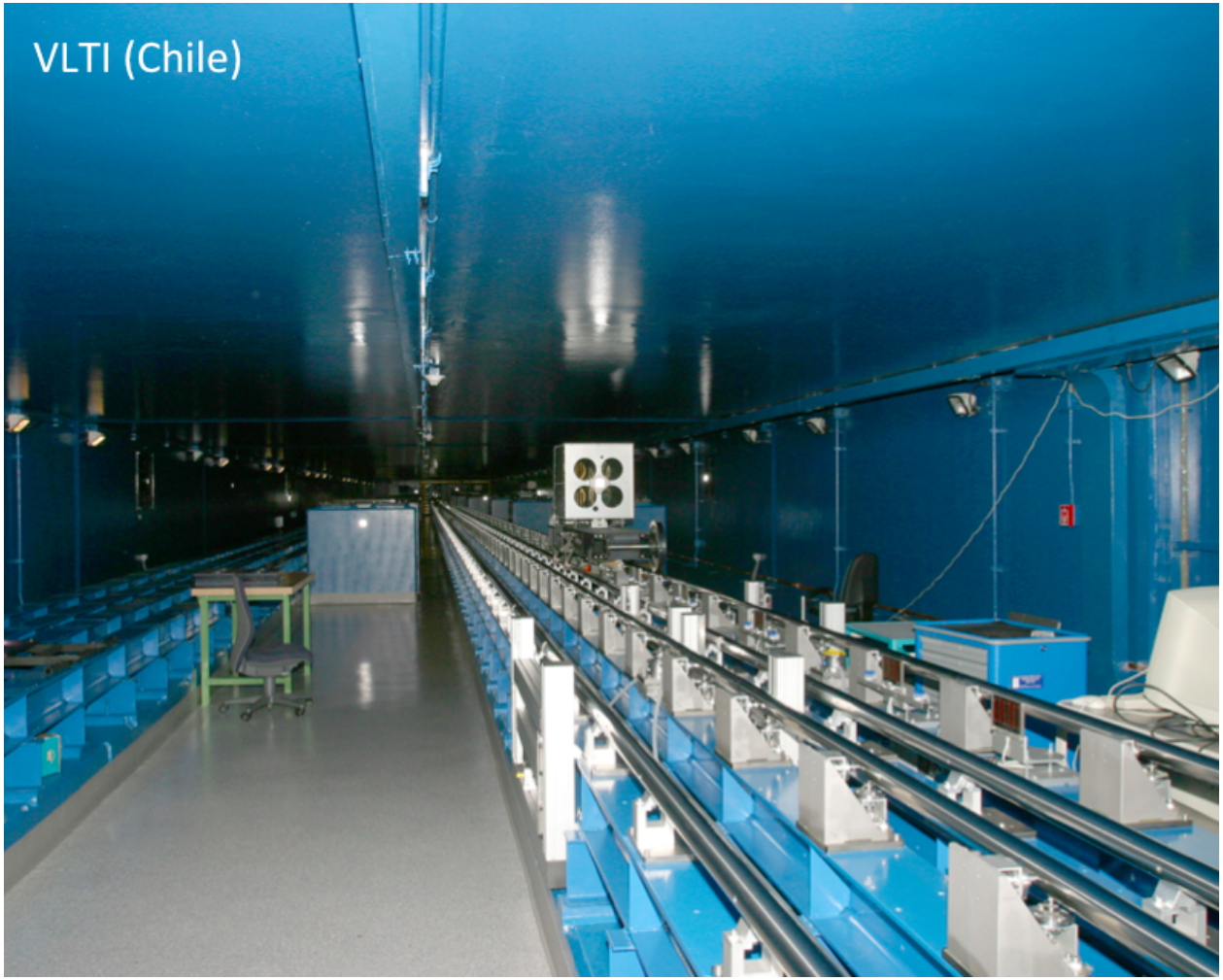

Figure: Optical delay lines at VLTI. © ESO.

Some examples of interferometers

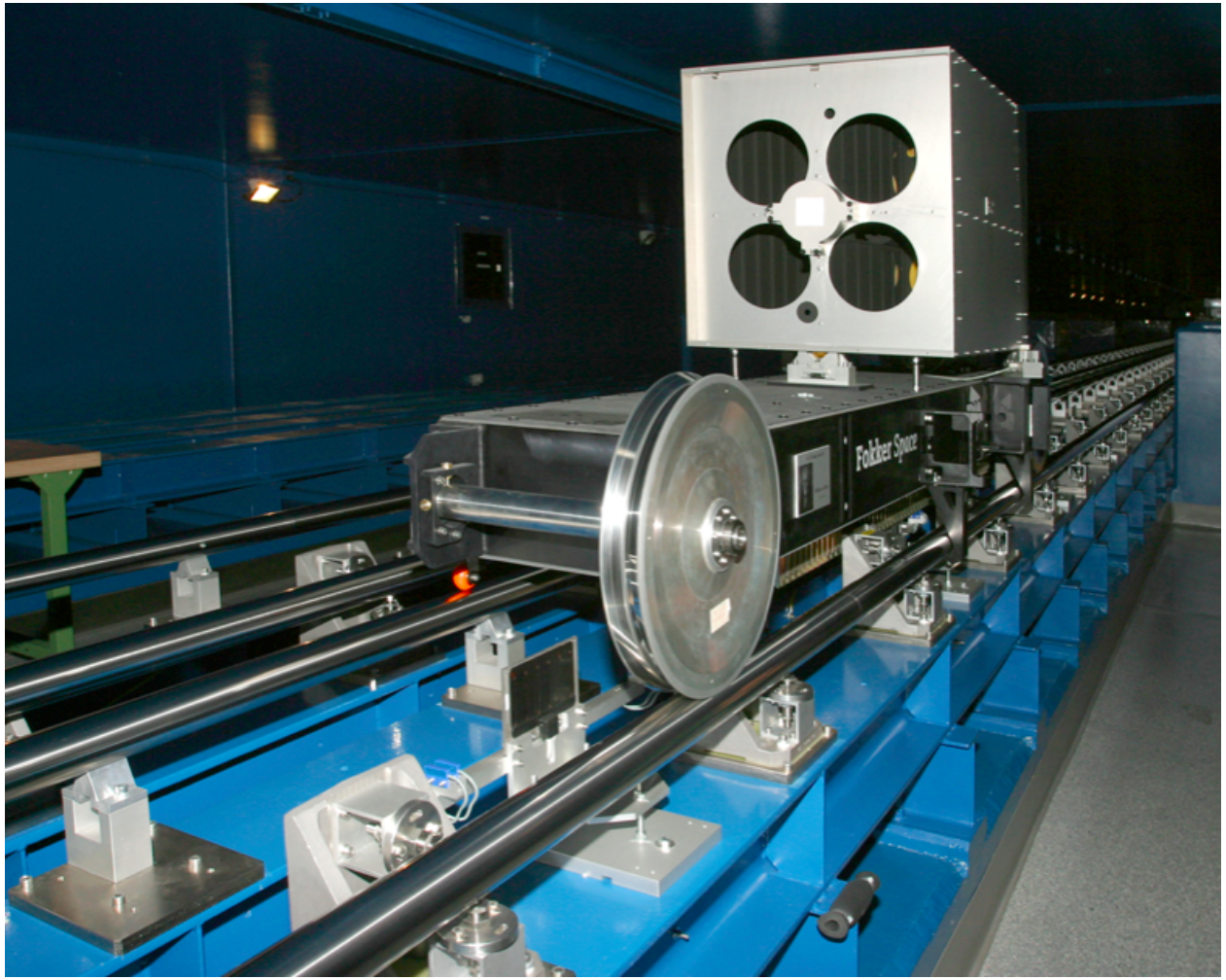

Figure: Optical delay lines at VLTI. © ESO.

Some examples of interferometers

The GI2T (in French, "Grand Interféromètre à 2 Télescopes") composed of two 1.5m telescopes was subsequently used by the same team. The two big telescopes could in principle be set 2 km apart, corresponding to an angular resolution $\Phi \sim 0.0001''$ for V_{lim} = 15-17 (see Fig. 31). Prof. A. Labeyrie also proposed to build a large network of ($\sim$ 27) optical telescopes whose individual diameters would be of the order of 10m.

Figure: The GI2T constructed by Antoine Labeyrie and his close collaborators on the plateau of Caussols, north of Grasse, near Nice (France, © Observatoire de la Côte d'Azur).

Some examples of interferometers

Since the beginning of the 21^{st} century, the modern sanctuary of stellar interferometry and aperture synthesis is undoubtedly the Very Large Telescope Interferometer (VLTI) of ESO (Southern European Observatory), located in Chile on Mount Paranal (see Fig. 32).

Some examples of interferometers

Since the beginning of the 21^{st} century, the modern sanctuary of stellar interferometry and aperture synthesis is undoubtedly the Very Large Telescope Interferometer (VLTI) of ESO (Southern European Observatory), located in Chile on Mount Paranal (see Fig. 32). The VLTI is a European interferometer that can re-combine the signal from 2, 3 or 4 telescopes depending on the instrument used. It has 4 telescopes of 8.2m and 4 mobile telescopes of 1.8m. Only telescopes of the same size can be re-combined together. The auxiliary telescopes of 1.8m can be easily moved allowing a better coverage of the u, v plane. The maximum base length of this interferometer is about 200m.

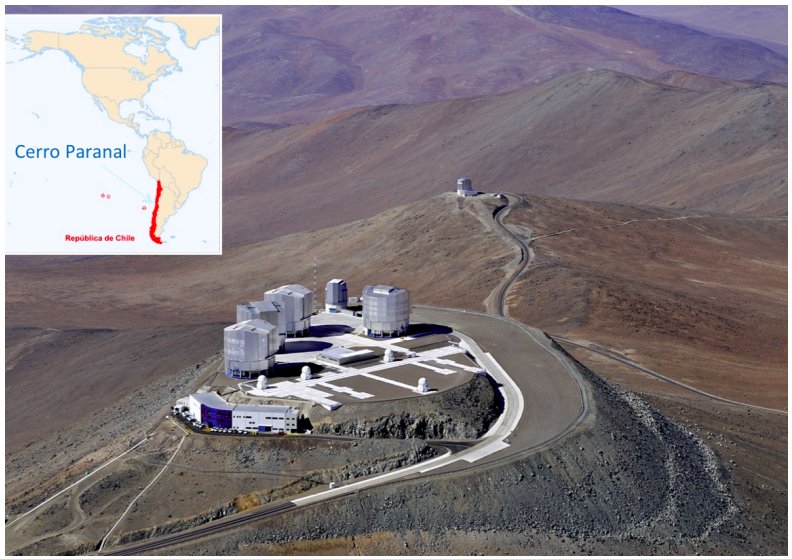

Figure: The Very Large Telescope Interferometer (VLTI) at the top ofParanal (Chile, © ESO).

Some examples of interferometers

CHARA is another very performing interferometer located on the heights of Los Angeles, California (see Fig. 33). It is installed on the historic observatory of Mount Wilson. Remember that it was with the 2.5m telescope of this observatory that the first measurement of a stellar diameter was made by Michelson and Pease by installing a beam of 7m at the top of the telescope.

Some examples of interferometers

CHARA is another very performing interferometer located on the heights of Los Angeles, California (see Fig. 33). It is installed on the historic observatory of Mount Wilson. Remember that it was with the 2.5m telescope of this observatory that the first measurement of a stellar diameter was made by Michelson and Pease by installing a beam of 7m at the top of the telescope.
The CHARA interferometric array, operational since 1999 is composed of 6 telescopes of 1m in diameter. These 6 telescopes can be either re-combined by 2, by 3 since 2008 and very soon the 6 together. The maximum base length of this interferometer is 330m allowing to achieve an angular resolution of 200μarcsec.

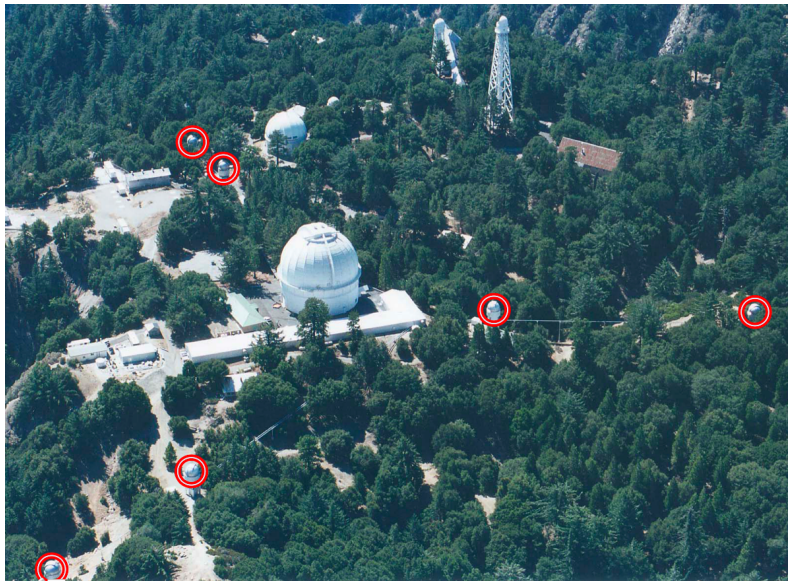

Figure: The CHARA interferometer composed of six 1m telescopes at Mount Wilson Observatory (California, USA). © The Observatories of the Carnegie Institution.

Some examples of interferometers

It is mainly used for angular diameter measurements but also for the detection and characterization of tight binary stars as well as for the detection of exo-zodiacal clouds (clouds of dust gravitating around the stars).

Some examples of interferometers

It is mainly used for angular diameter measurements but also for the detection and characterization of tight binary stars as well as for the detection of exo-zodiacal clouds (clouds of dust gravitating around the stars).
Another famous optical/IR interferometer is the Keck Interferometer made of two 10m telescopes separated by a fixed baseline of 85m (see Fig. 34) on top of Mauna Kea (Hawaii, USA).

Figure: The Keck interferometer on top of Mauna Kea (Hawaii, USA). © Ethan Tweedie.

Table of Contents

Two important theorems and some applications: the fundamental theorem

When we previously established the relation existing between the structure of an extended celestial source and the visibility of the fringes observed with an interferometer, we implicitly assumed that the size of the apertures was infinitely small (hole apertures).

Two important theorems and some applications: the fundamental theorem

When we previously established the relation existing between the structure of an extended celestial source and the visibility of the fringes observed with an interferometer, we implicitly assumed that the size of the apertures was infinitely small (hole apertures). Use of the fundamental theorem allows one to calculate the response function of an interferometer equipped with finite size apertures.

Two important theorems and some applications: the fundamental theorem

When we previously established the relation existing between the structure of an extended celestial source and the visibility of the fringes observed with an interferometer, we implicitly assumed that the size of the apertures was infinitely small (hole apertures). Use of the fundamental theorem allows one to calculate the response function of an interferometer equipped with finite size apertures.

The fundamental theorem that we demonstrate in the lecture notes merely stipulates that given a converging optical system which can be assimilated to the lens or to the mirror of a telescope, or of an optical interferometer, the complex amplitude distribution $a(p, q)$ of the electromagnetic field of radiation in the focal plane is the Fourier transform of the complex amplitude distribution $A(x, y)$ of the electromagnetic field in the pupil plane, i.e.

$$a(p, q) = \int_{R^2} A(x, y) \exp\left[-i2\pi(px + qy)\right] dxdy \tag{40}$$

Two important theorems and some applications: the fundamental theorem

When we previously established the relation existing between the structure of an extended celestial source and the visibility of the fringes observed with an interferometer, we implicitly assumed that the size of the apertures was infinitely small (hole apertures). Use of the fundamental theorem allows one to calculate the response function of an interferometer equipped with finite size apertures.

The fundamental theorem that we demonstrate in the lecture notes merely stipulates that given a converging optical system which can be assimilated to the lens or to the mirror of a telescope, or of an optical interferometer, the complex amplitude distribution $a(p,q)$ of the electromagnetic field of radiation in the focal plane is the Fourier transform of the complex amplitude distribution $A(x,y)$ of the electromagnetic field in the pupil plane, i.e.

$$a(p,q) = \int_{R^2} A(x,y) \exp\left[-i2\pi(px+qy)\right] dxdy \tag{40}$$

or in a more compact form

$$a(p,q) = FT_{-}(A(x,y))(p,q) \tag{41}$$

with

$$p = \frac{x'}{\lambda f} \quad \text{and} \quad q = \frac{y'}{\lambda f} \tag{42}$$

where x', y' refer to the Cartesian coordinates in the focal plane, λ to the wavelength of the monochromatic light under consideration and f the effective focal length of the converging system.

where x', y' refer to the Cartesian coordinates in the focal plane, λ to the wavelength of the monochromatic light under consideration and f the effective focal length of the converging system.

Applications of the fundamental theorem: the case of a single square aperture

Adopting the definition (10) for the intensity of the vibrations, we find that (see Fig. 35, at right)

$$i(p,q) = a(p,q)\, a^*(p,q) = |a(p,q)|^2 = i_0\, a^4 \left(\frac{sin(\pi ap)}{\pi ap}\right)^2 \left(\frac{sin(\pi aq)}{\pi aq}\right)^2. \qquad (43)$$

Applications of the fundamental theorem: the case of a single square aperture

Adopting the definition (10) for the intensity of the vibrations, we find that (see Fig. 35, at right)

$$i(p,q) = a(p,q)\, a^*(p,q) = |a(p,q)|^2 = i_0\, a^4 \left(\frac{sin(\pi ap)}{\pi ap}\right)^2 \left(\frac{sin(\pi aq)}{\pi aq}\right)^2 . \qquad (43)$$

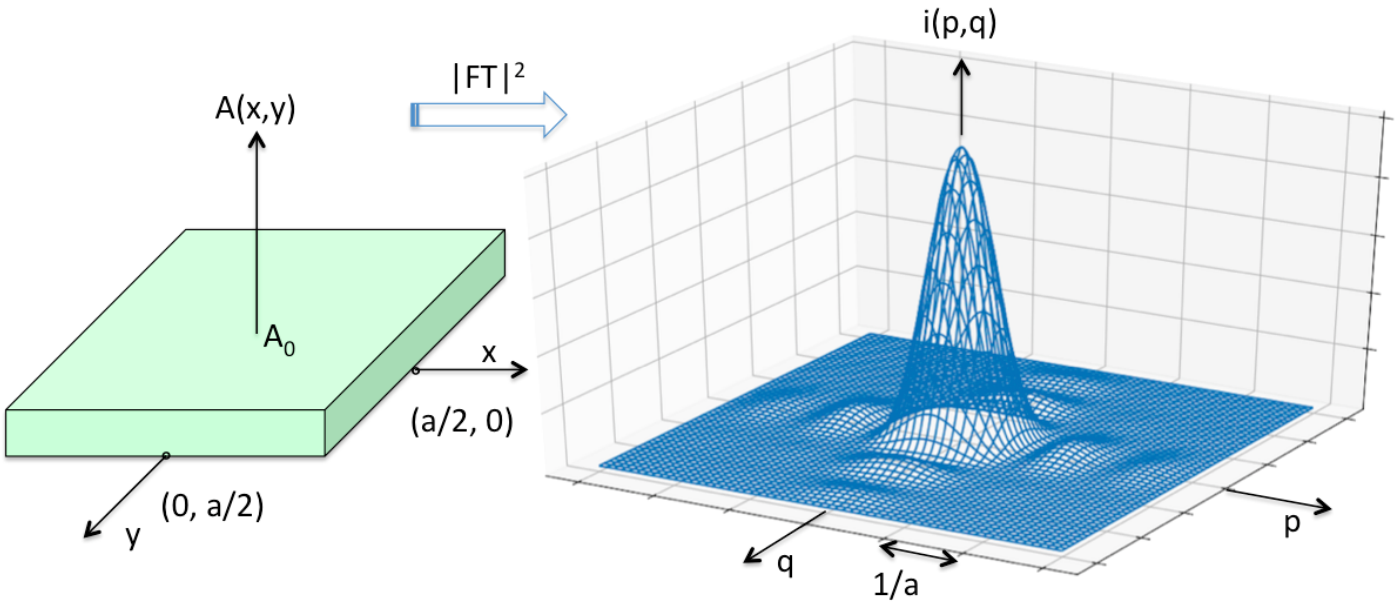

Figure: Complex amplitude distribution $A(x, y)$ in the plane of a single square aperture (left) and resulting response function in intensity $i(p, q)$ (right).

Applications of the fundamental theorem: the case of a single square aperture

Defining the angular resolution Φ of an optical system as being the angular width of the response function in intensity inside the first minima, we obtain for the values of $\pi pa = \pm\pi$ (resp. $\pi qa = \pm\pi$), i.e. $p = \pm 1/a$ (resp. $q = \pm 1/a$) and with the definition (42) for p, q

$$\frac{x'}{\lambda f} = \pm\frac{1}{a} \quad (\text{resp.} \quad \frac{y'}{\lambda f} = \pm\frac{1}{a}), \tag{44}$$

Applications of the fundamental theorem: the case of a single square aperture

Defining the angular resolution Φ of an optical system as being the angular width of the response function in intensity inside the first minima, we obtain for the values of $\pi pa = \pm\pi$ (resp. $\pi qa = \pm\pi$), i.e. $p = \pm 1/a$ (resp. $q = \pm 1/a$) and with the definition (42) for p, q

$$\frac{x'}{\lambda f} = \pm\frac{1}{a} \quad (\text{resp.} \quad \frac{y'}{\lambda f} = \pm\frac{1}{a}), \tag{44}$$

$$\Phi = \frac{\Delta x'}{f} = \frac{\Delta y'}{f} = \frac{2\lambda}{a}. \tag{45}$$

Applications of the fundamental theorem: the case of a single square aperture

Defining the angular resolution Φ of an optical system as being the angular width of the response function in intensity inside the first minima, we obtain for the values of $\pi pa = \pm\pi$ (resp. $\pi qa = \pm\pi$), i.e. $p = \pm 1/a$ (resp. $q = \pm 1/a$) and with the definition (42) for p, q

$$\frac{x'}{\lambda f} = \pm\frac{1}{a} \quad (\text{resp.} \quad \frac{y'}{\lambda f} = \pm\frac{1}{a}), \tag{44}$$

$$\Phi = \frac{\Delta x'}{f} = \frac{\Delta y'}{f} = \frac{2\lambda}{a}. \tag{45}$$

The angular resolution is thus inversely proportional to the size a of the square aperture, and proportional to the wavelength λ. Working at short wavelength with a big size aperture thus confers a better angular resolution.

Applications of the fundamental theorem: the case of a single square aperture

Defining the angular resolution Φ of an optical system as being the angular width of the response function in intensity inside the first minima, we obtain for the values of $\pi pa = \pm\pi$ (resp. $\pi qa = \pm\pi$), i.e. $p = \pm 1/a$ (resp. $q = \pm 1/a$) and with the definition (42) for p, q

$$\frac{x'}{\lambda f} = \pm\frac{1}{a} \quad (\text{resp.} \quad \frac{y'}{\lambda f} = \pm\frac{1}{a}), \tag{44}$$

$$\Phi = \frac{\Delta x'}{f} = \frac{\Delta y'}{f} = \frac{2\lambda}{a}. \tag{45}$$

The angular resolution is thus inversely proportional to the size a of the square aperture, and proportional to the wavelength λ. Working at short wavelength with a big size aperture thus confers a better angular resolution.

Two important theorems and some applications: the two telescope interferometer

Figure 36 (upper left) illustrates the principle of optically coupling two telescopes. Such a system is equivalent to a huge telescope in front of which would have been placed a screen pierced with two openings corresponding to the entrance pupils of the two telescopes. The pupil function $A(x, y)$ of this system is shown in that same Figure for the case of two square apertures.

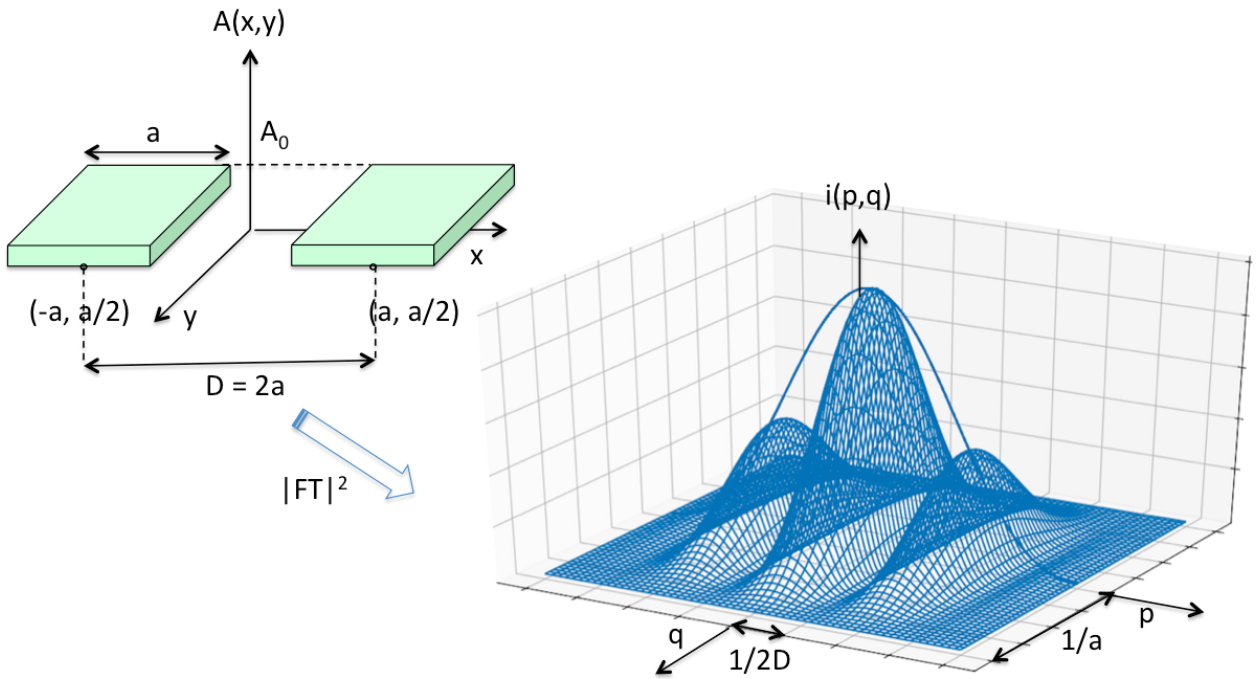

Figure: The two telescope interferometer: distribution of the complex amplitude for the case of two square apertures (upper left) and the corresponding impulse response function (lower right).

Two important theorems and some applications: the two telescope interferometer

Let us now calculate the impulse response function $a(p, q)$ of such a system.

Two important theorems and some applications: the two telescope interferometer

Let us now calculate the impulse response function $a(p, q)$ of such a system. Representing the distribution of the complex amplitude over each of the individual square apertures by means of the function $A_0(x, y)$ and assuming that the distance between their optical axes is D, we find that

$$a(p, q) = FT_{-}[A_0(x + D/2, y) + A_0(x - D/2, y)](p, q). \tag{46}$$

Two important theorems and some applications: the two telescope interferometer

Let us now calculate the impulse response function $a(p,q)$ of such a system. Representing the distribution of the complex amplitude over each of the individual square apertures by means of the function $A_0(x,y)$ and assuming that the distance between their optical axes is D, we find that

$$a(p,q) = FT_{-}[A_0(x+D/2,y) + A_0(x-D/2,y)](p,q). \tag{46}$$

It is easy to show that the previous equation may reduce to

$$a(p,q) = [\exp(i\pi pD) + \exp(-i\pi pD)]\, FT_{-}[A_0(x,y)](p,q), \tag{47}$$

$$a(p,q) = 2\, cos(\pi pD)\, FT_{-}[A_0(x,y)](p,q) \tag{48}$$

and finally

$$i(p,q) = a(p,q)a^{*}(p,q) = |a(p,q)|^2 = 4\, cos^2(\pi pD)\, \{FT_{-}[A_0(x,y)](p,q)\}^2. \tag{49}$$

Two important theorems and some applications: the two telescope interferometer

Let us now calculate the impulse response function $a(p,q)$ of such a system. Representing the distribution of the complex amplitude over each of the individual square apertures by means of the function $A_0(x,y)$ and assuming that the distance between their optical axes is D, we find that

$$a(p,q) = FT_{-}[A_0(x+D/2,y) + A_0(x-D/2,y)](p,q). \tag{46}$$

It is easy to show that the previous equation may reduce to

$$a(p,q) = [\exp(i\pi pD) + \exp(-i\pi pD)]\, FT_{-}[A_0(x,y)](p,q), \tag{47}$$

$$a(p,q) = 2\, cos(\pi pD)\, FT_{-}[A_0(x,y)](p,q) \tag{48}$$

and finally

$$i(p,q) = a(p,q)a^{*}(p,q) = |a(p,q)|^2 = 4\, cos^2(\pi pD)\, \{FT_{-}[A_0(x,y)](p,q)\}^2. \tag{49}$$

Particularizing this intensity distribution to the case of two square apertures and making use of the relation (43) leads to the result

$$i(p,q) = A_0^2\,(2a^2)^2\,[\frac{sin(\pi pa)}{\pi pa}]^2\,[\frac{sin(\pi qa)}{\pi qa}]^2\,cos^2(\pi pD). \tag{50}$$

Particularizing this intensity distribution to the case of two square apertures and making use of the relation (43) leads to the result

$$i(p,q) = A_0^2\,(2a^2)^2\,[\frac{sin(\pi pa)}{\pi pa}]^2\,[\frac{sin(\pi qa)}{\pi qa}]^2\,cos^2(\pi pD). \qquad (50)$$

Figure 36 (lower right) illustrates the response function for the latter case. We see that the impulse response of each individual telescope is modulated by the $\cos(2\pi pD)$ function and that the resulting impulse response function shows consequently a more detailed structure along the p axis, leading to a significantly improved angular resolution Φ along that direction.

Particularizing this intensity distribution to the case of two square apertures and making use of the relation (43) leads to the result

$$i(p,q) = A_0^2\,(2a^2)^2\,[\frac{sin(\pi pa)}{\pi pa}]^2\,[\frac{sin(\pi qa)}{\pi qa}]^2\,cos^2(\pi pD). \tag{50}$$

Figure 36 (lower right) illustrates the response function for the latter case. We see that the impulse response of each individual telescope is modulated by the $\cos(2\pi pD)$ function and that the resulting impulse response function shows consequently a more detailed structure along the p axis, leading to a significantly improved angular resolution Φ along that direction.

The angular width Φ of the bright central fringe is equal to the angular width separating the two minima located on its two sides. We thus find successively

$$\pi pD = \pm\frac{\pi}{2}, \tag{51}$$

$$p = \pm \frac{1}{2D}, \tag{52}$$

$$\Delta p = \frac{1}{D} \tag{53}$$

and making use of relation (42)

$$\Phi = \frac{\Delta x'}{f} = \frac{\lambda}{D}. \tag{54}$$

$$p = \pm \frac{1}{2D}, \tag{52}$$

$$\Delta p = \frac{1}{D} \tag{53}$$

and making use of relation (42)

$$\Phi = \frac{\Delta x'}{f} = \frac{\lambda}{D}. \tag{54}$$

The angular resolution of the interferometer along the direction joining the two telescopes is approximately equivalent to that of a single dish telescope which diameter is equal to the baseline D separating them, and not any longer to the diameter of each single telescope (see Eqs. (45) or (**??**)).

The convolution theorem states that the convolution of two functions $f(x)$ and $g(x)$ is given by the following expression

$$f(x) * g(x) = (f * g)(x) = \int_R f(x-t)g(t)dt. \tag{55}$$

Figure 37 illustrates such a convolution product for the case of two rectangular functions $f(x) = \Pi(x/a)$ and $g(x) = \Pi(x/b)$ having the widths a and b, respectively.

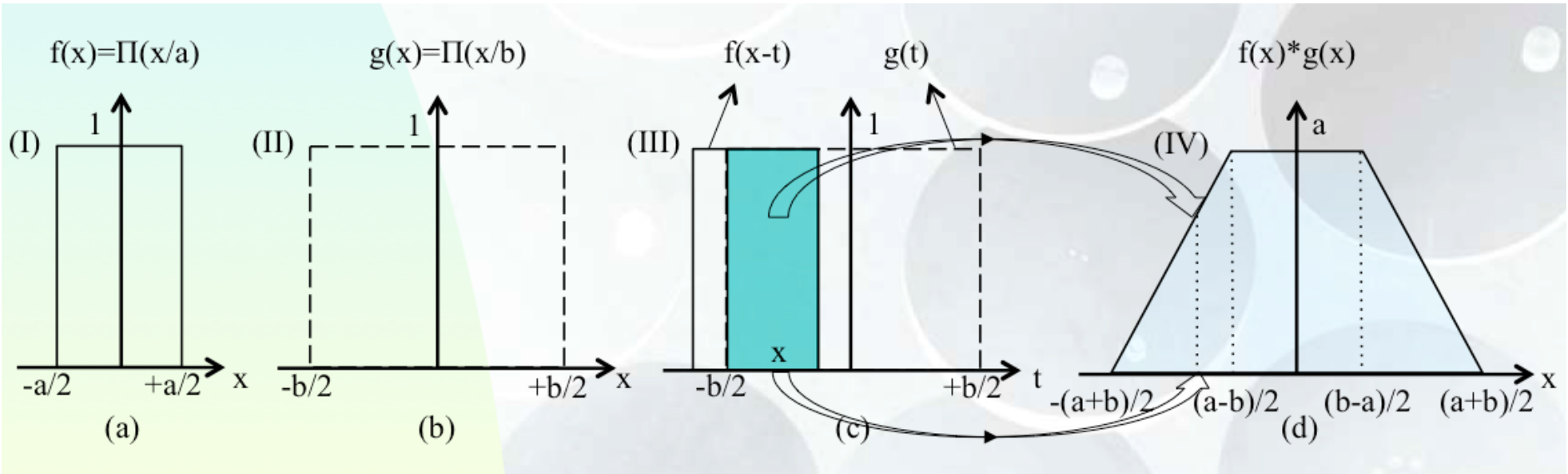

Figure: Convolution product of two 1-D rectangular functions. (a) $f(x)$, (b) $g(x)$, (c) $g(t)$ and $f(x-t)$. The dashed area represents the integral of the product of $f(x-t)$ and $g(t)$ for the given x offset, (d) $f(x) * g(x) = (f * g)(x)$ represents the previous integral as a function of x.

Two important theorems and some applications: the convolution theorem

Every day when the Sun is shining, it is possible to see nice illustrations of the convolution product while looking at the projected images of the Sun on the ground which are actually produced through small holes in the foliage of the trees (see the illustration in Fig. 38). It is a good exercise to establish the relation existing between the observed surface brightness of those Sun images, the shape of the holes in the foliage of the trees, their distance from the ground and the intrinsic surface brightness distribution of the Sun.

Figure: Projected images of the Sun on the ground actually produced through small holes in the foliage of trees (bamboo trees at IUCAA, Pune, India, June 2016). These images actually result from the convolution of the intrinsic Sun intensity distribution and the shapes of the holes in the trees.

References

These lecture notes are based upon lectures on the same subject delivered by the author in French at the Liège University during the past ten years (see [1]). To get deeper into the field of interferometry, we highly recommend the following books: [2], [3], [4].

1. J. Surdej, see http://www.aeos.ulg.ac.be/teaching.php (2018)
2. P. Léna, D. Rouan, F., Lebrun, F. Mignard, D., Pelat, D., *Observational Astrophysics* (Astronomy and Astrophysics Library, 2012)
3. A. Glindemann, *Principles of Stellar Interferometry* (Astronomy and Astrophysics Library, 2011)
4. D. Buscher, *Practical Optical Interferometry: Imaging at Visible and Infrared Wavelengths* (Cambridge University Press, 2015)